Electronic Supplementary Material (ESI) for CrystEngComm.

Modulation of Supramolecular Self-Assembly of BODIPY Tectons via Halogen Bonding

Emrah Özcan,[a,b] Burcu Dedeoglu,[a] Yurii Chumakov,[c,d] Yunus Zorlu,[a] Bünyemin Çoşut,[a] Mehmet Menaf Ayhan*[a]

[a] Department of Chemistry, Gebze Technical University, Gebze, Kocaeli,41400 Turkey

[b] Institute of Physics, Faculty of Science, University of South Bohemia, Branišovská 1760, 370 05, České Budějovice, Czech Republic

[c] Department of Physics, Gebze Technical University, Gebze, Kocaeli, 41400 Turkey

[d] Institute of Applied Physics, MD-2028, Chisinau, Moldova

* Author for correspondence: menafayhan@gtu.edu.tr

TABLE OF CONTENTS

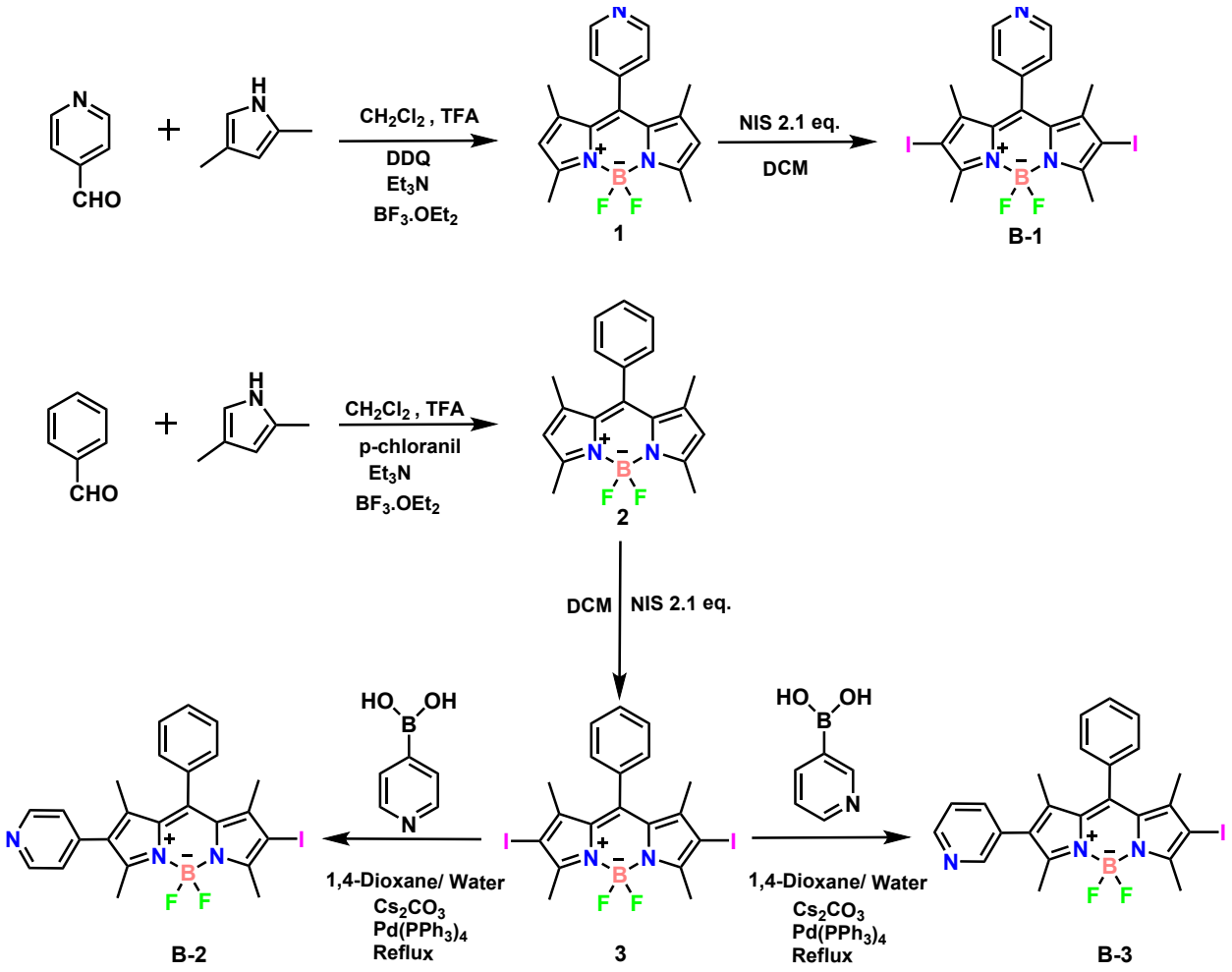

Scheme 1. Synthetic pathway of compounds **1-3** and **B-1, B-2,** and **B-3**

1. Experimental Section

1.1. Materials and Methods

All chemicals and solvents were purchased from Sigma Aldrich and TCI Chemicals used as supplied without further purification unless stated otherwise. NMR spectra were recorded on a Bruker 400 spectrometer (^{1}H, 500 MHz; ^{13}C, 125 MHz). MALDI-TOF was performed on a Bruker Microflex LT MALDI-TOF-MS Instrument.

1.1. 2. X-ray Crystallography

Single crystal data were collected on a Bruker APEX II QUAZAR three-circle diffractometer. Indexing was performed using APEX2.[55] Data integration and reduction was carried out with SAINT.[56] Absorption correction was performed by multi-scan method implemented in SADABS.[57] The structure was solved using SHELXT[58] and then refined by full-matrix least-squares refinements on F^2 using the SHELXL[58] in Olex2 Software Package.[59] Aromatic and aliphatic C-bound H atoms were positioned geometrically and refined using a riding mode. One entire BODIPY molecule in the asymmetric unit of **B-2** is disordered over two sites with occupancies 0.84:0.16. Crystal structure validations, geometrical calculations and crystal packing analysis were performed using Platon software.[60] The molecular drawings were carried out with Mercury CSD program.[61]

2. Synthesis

The compounds 1, 2 and 3 were synthesized and purified according to literature.[1,2] Compounds B-1, B-2 and B-3 were prepared with modified methods described in literature. [3,4]

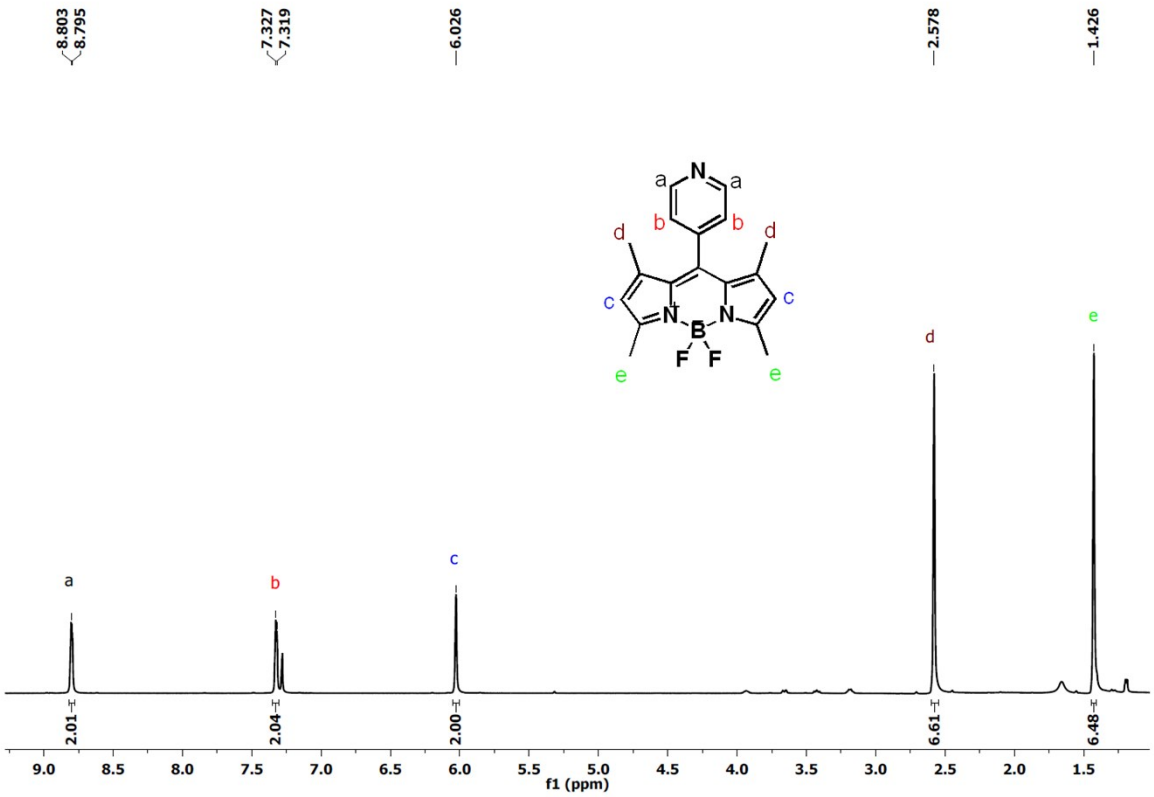

Figure S1. ^{1}H NMR Spectrum of Compound **1**

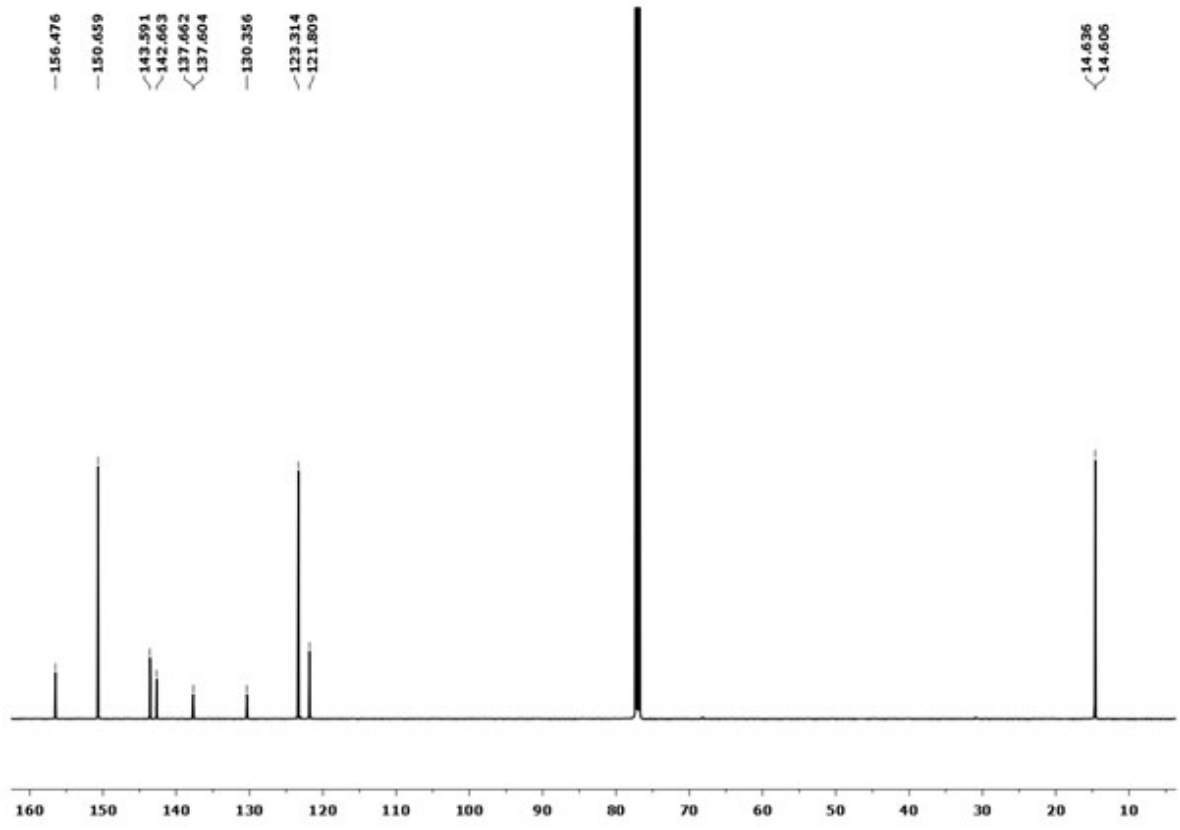

Figure S2. ^{13}C NMR Spectrum of Compound **1**

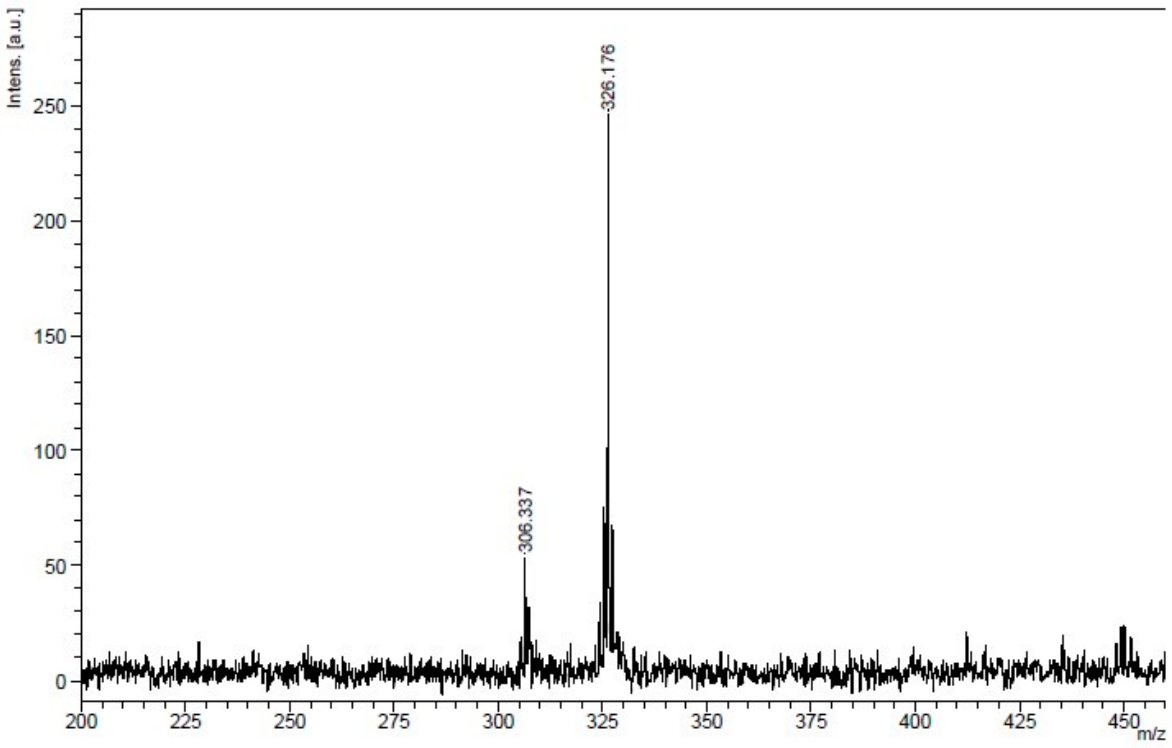

Figure S3. Mass Spectrum of Compound **1**

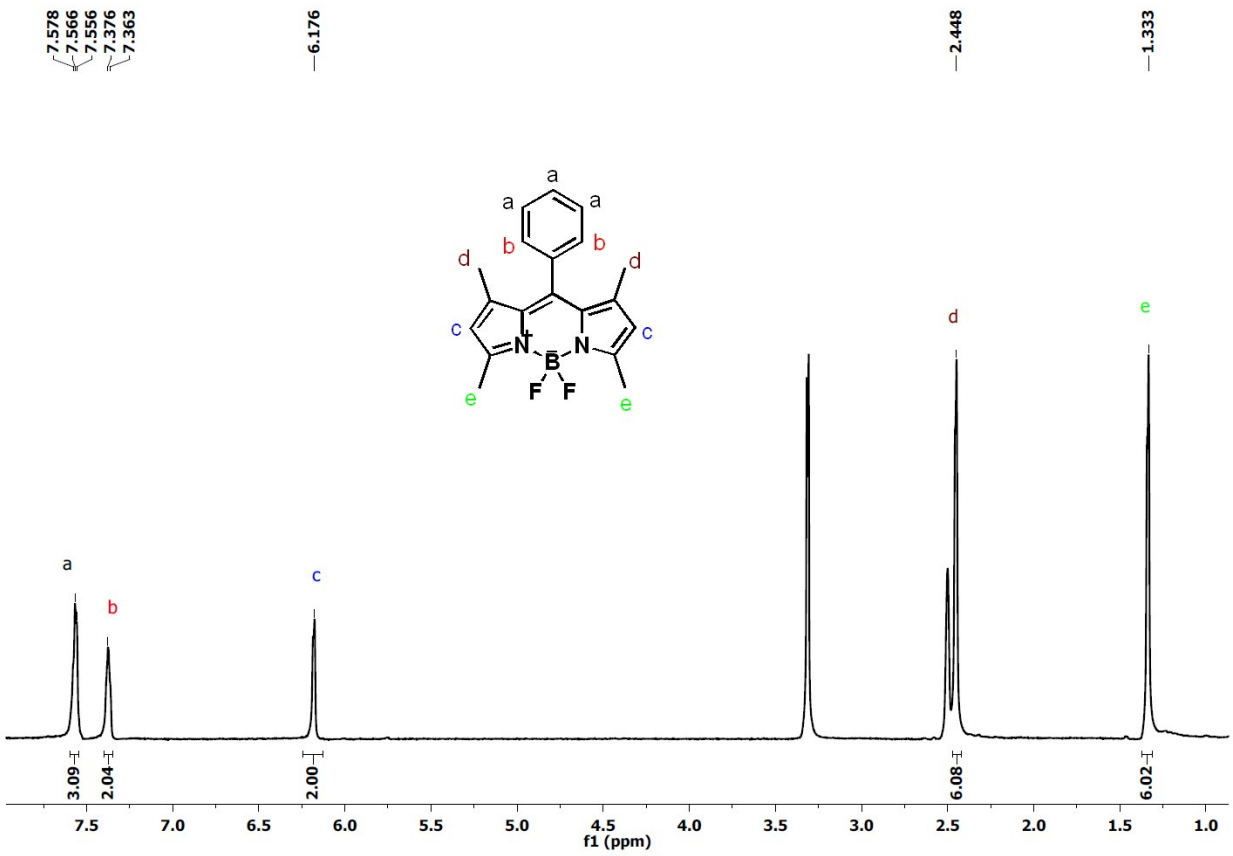

Figure S4. [1]H NMR Spectrum of Compound **2**

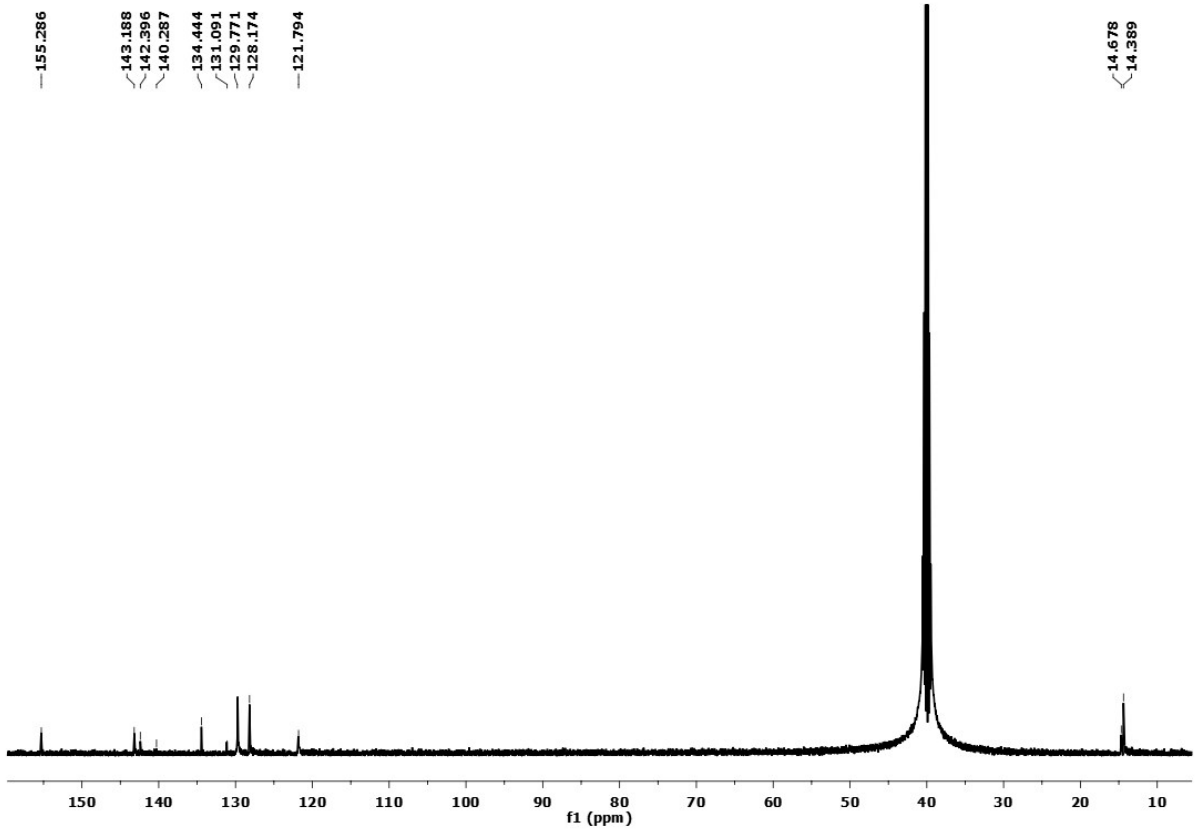

Figure S5. ^{13}C NMR Spectrum of Compound **2**

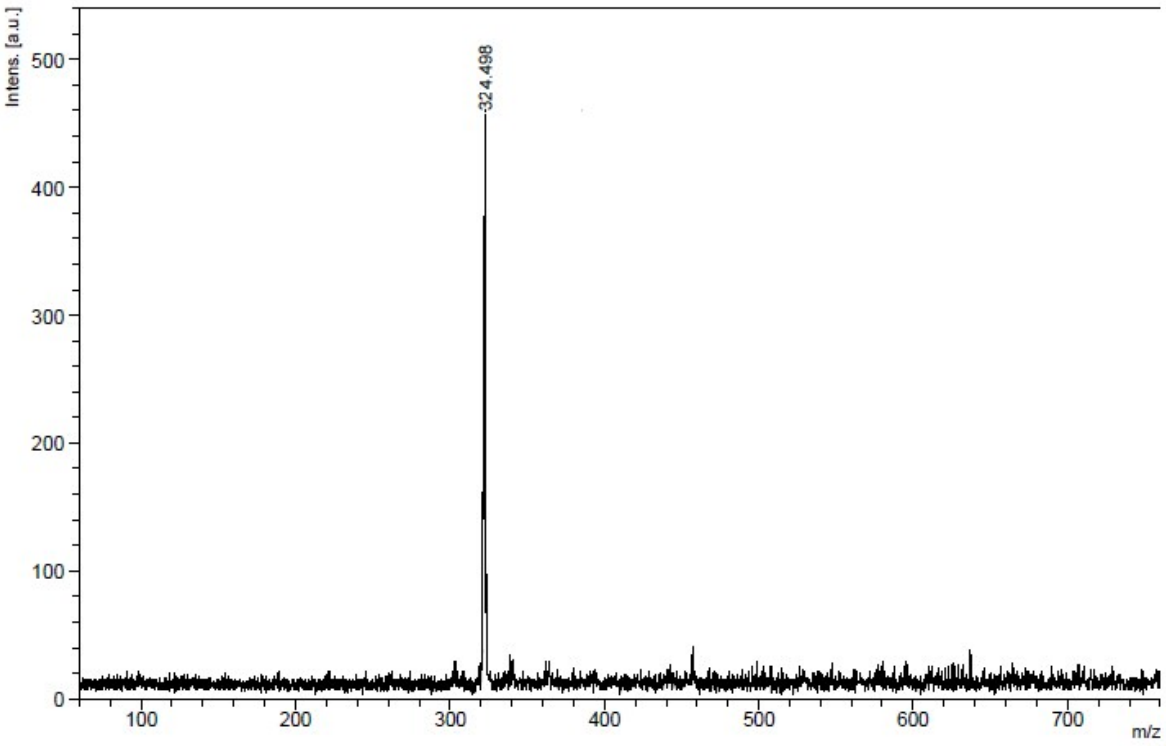

Figure S6. Mass Spectrum of Compound **2**

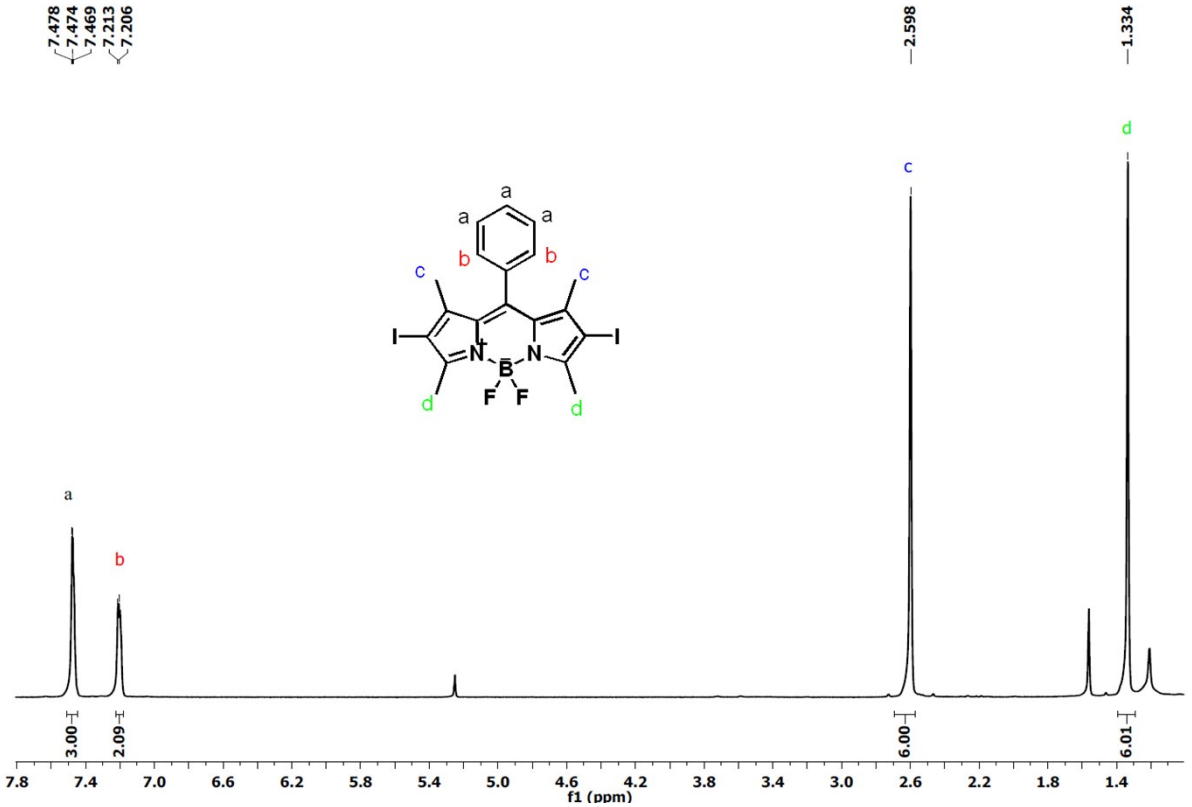

Figure S7. ^{1}H NMR Spectrum of Compound **3**

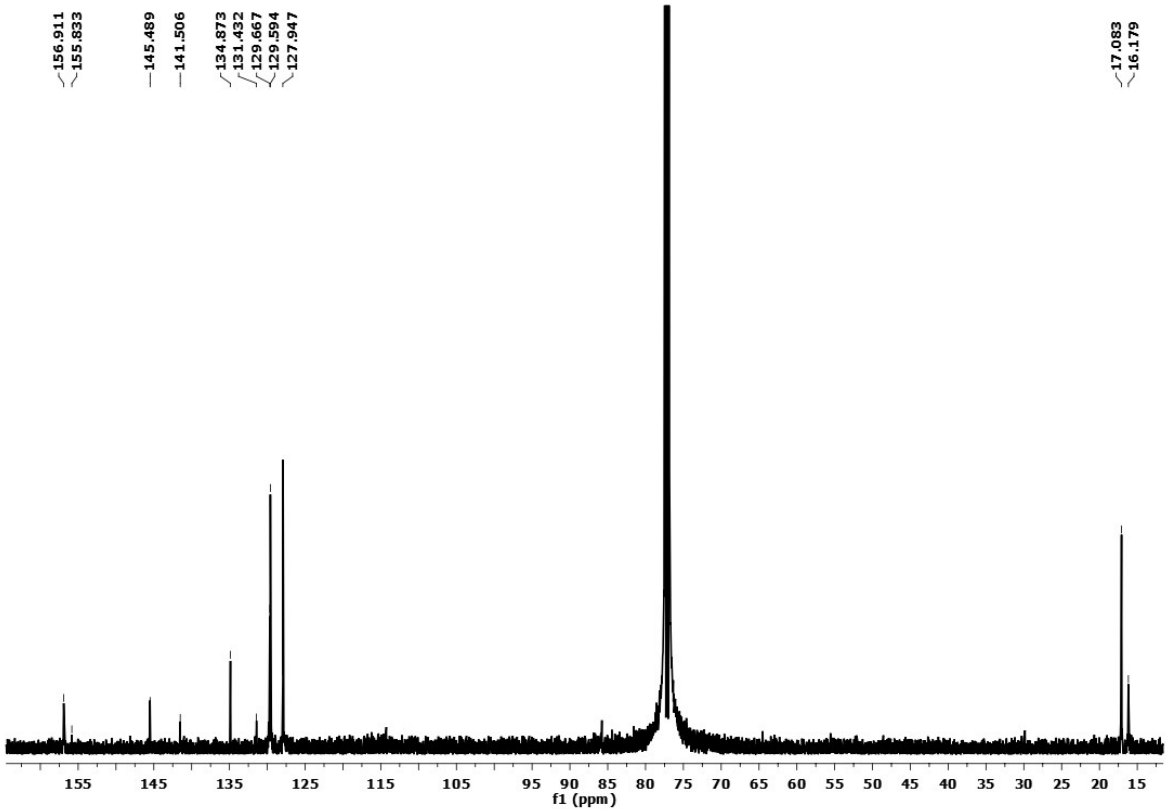

Figure S8. ^{13}C NMR Spectrum of Compound **3**

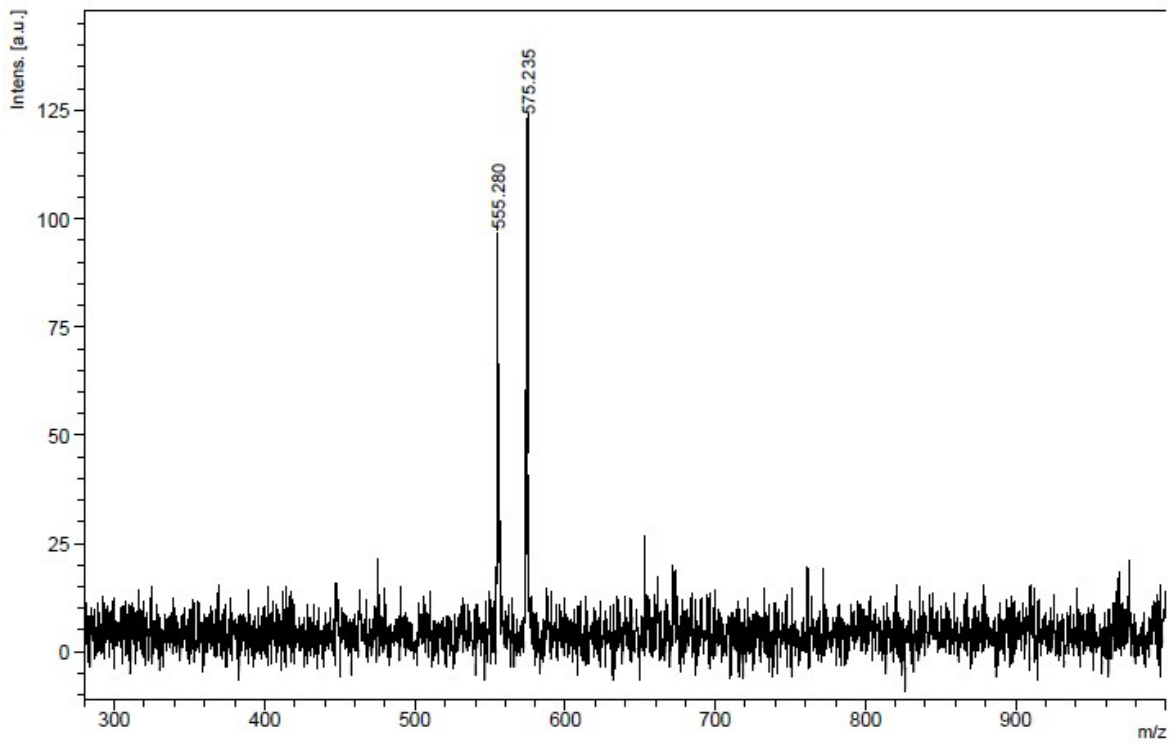

Figure S9. Mass Spectrum of Compound **3**

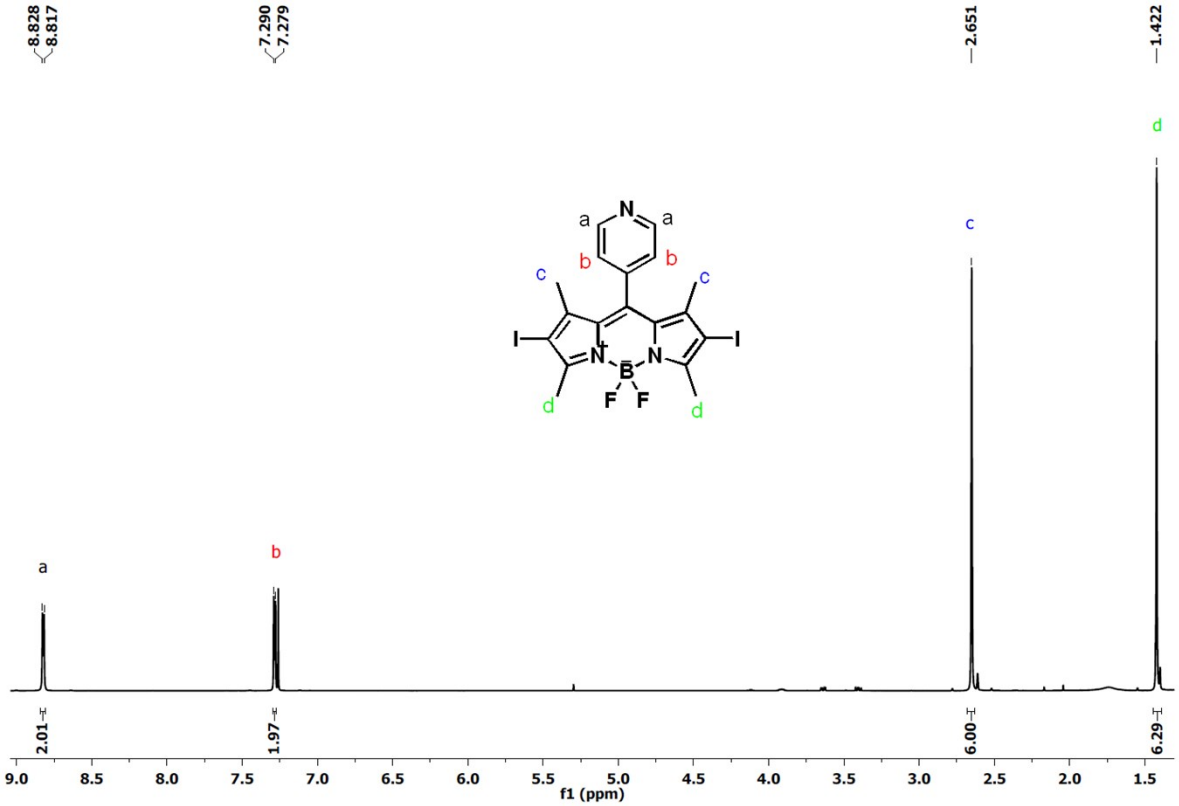

Figure S10. ^{1}H NMR Spectrum of Compound **B-1**

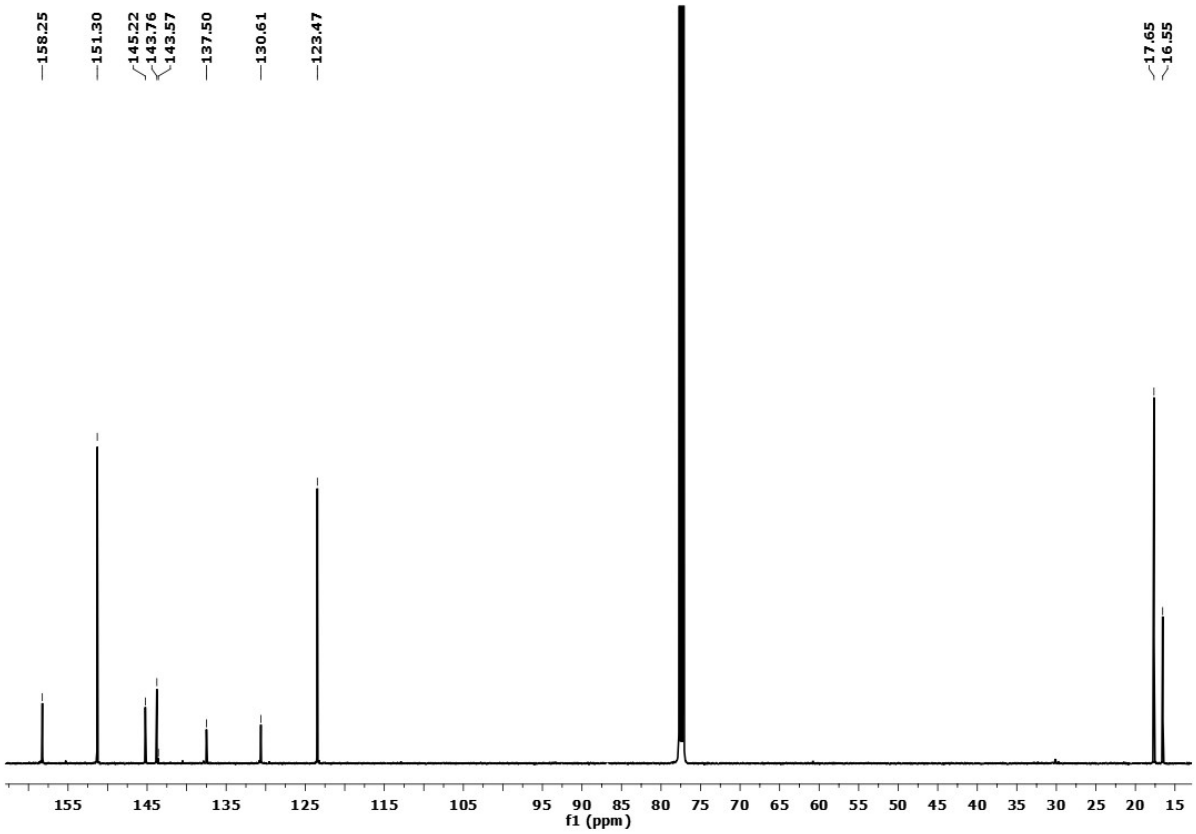

Figure S11. ^{13}C NMR Spectrum of Compound **B-1**

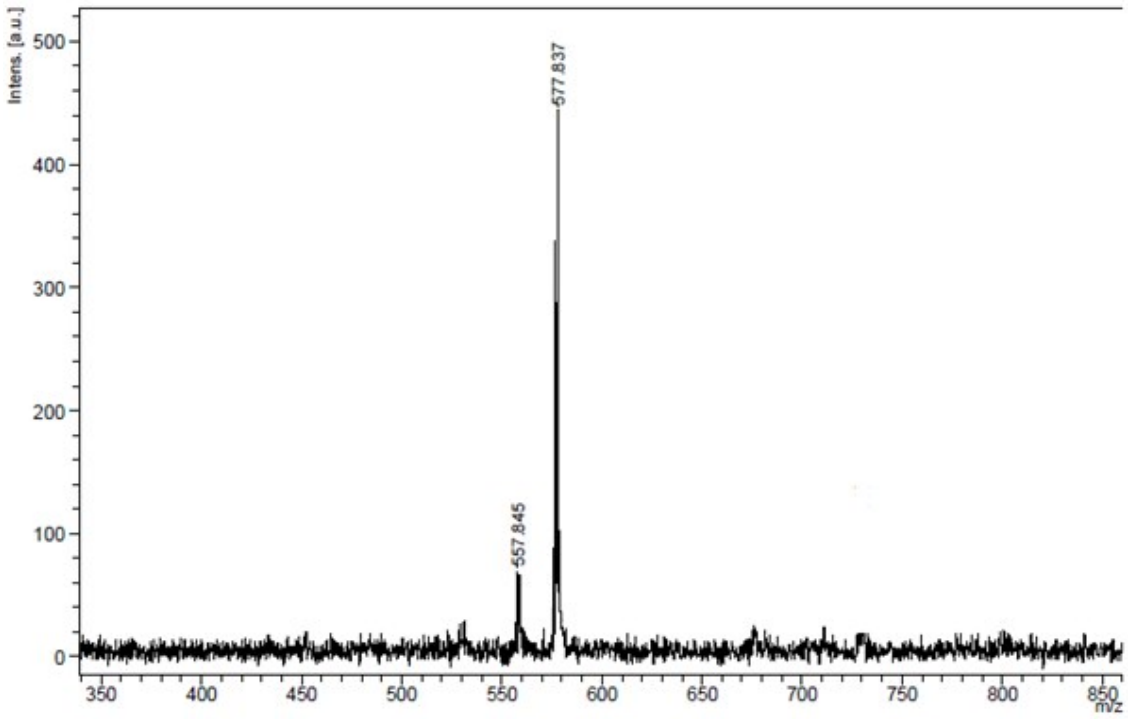

Figure S12. Mass Spectrum of Compound **B-1**

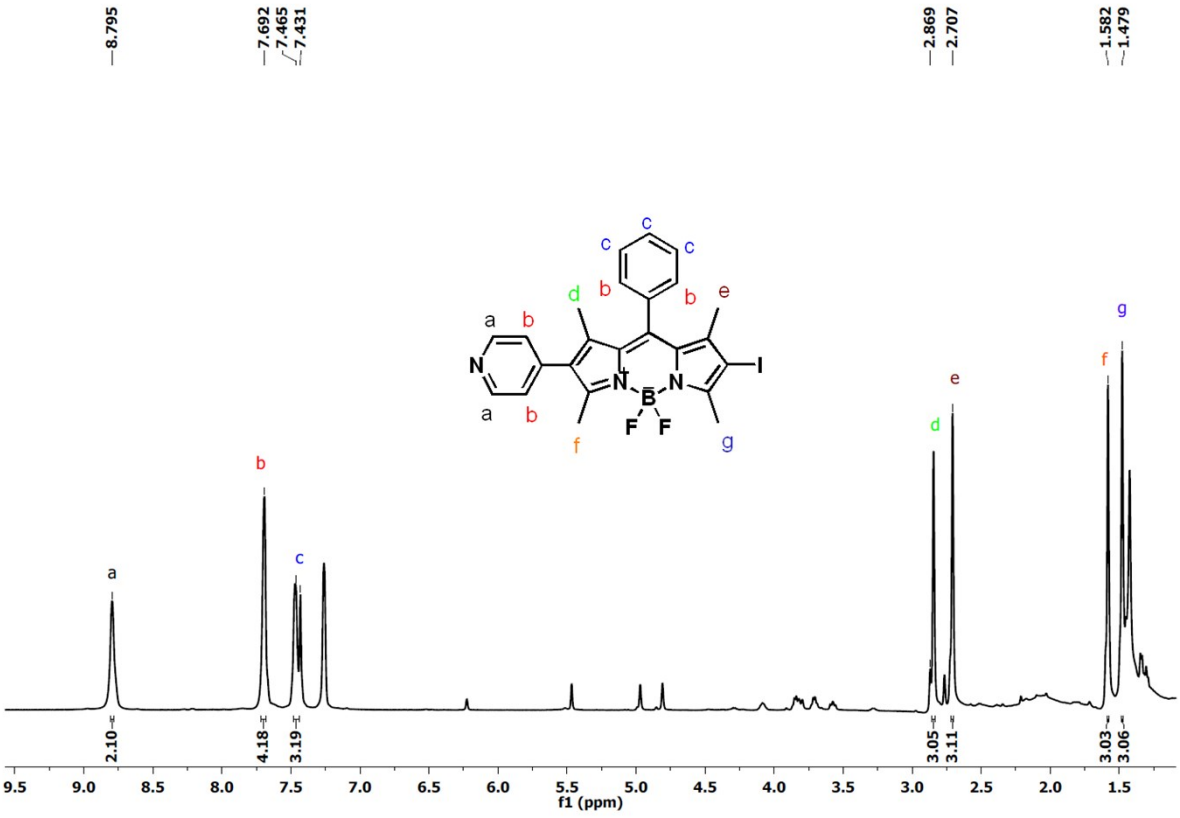

Figure S13. ^{1}H NMR Spectrum of Compound **B-2**

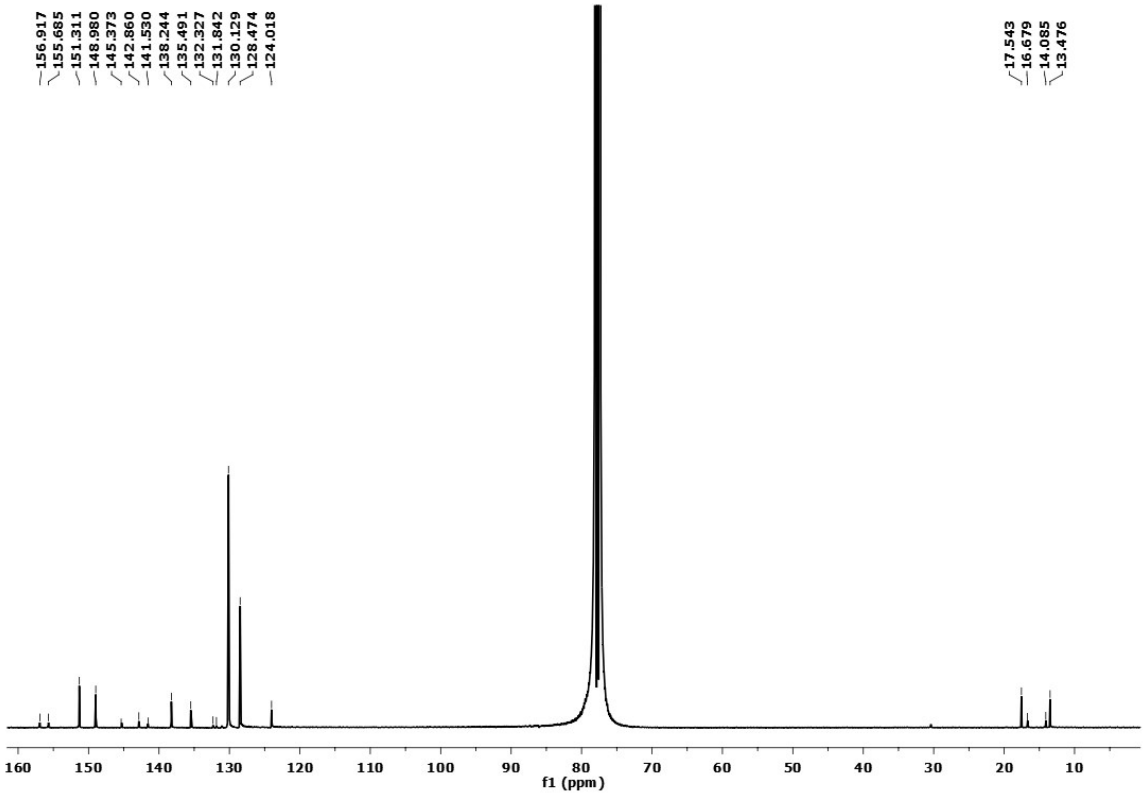

Figure S14. ^{13}C NMR Spectrum of Compound **B-2**

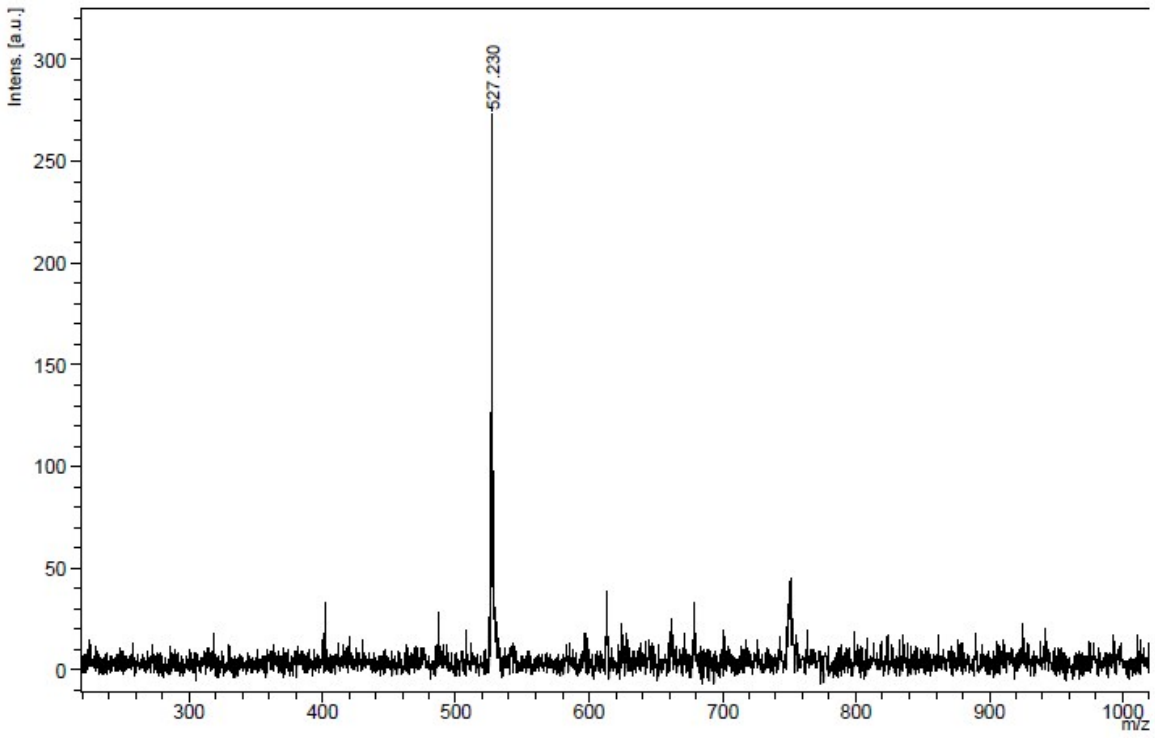

Figure S15. Mass Spectrum of Compound **B-2**

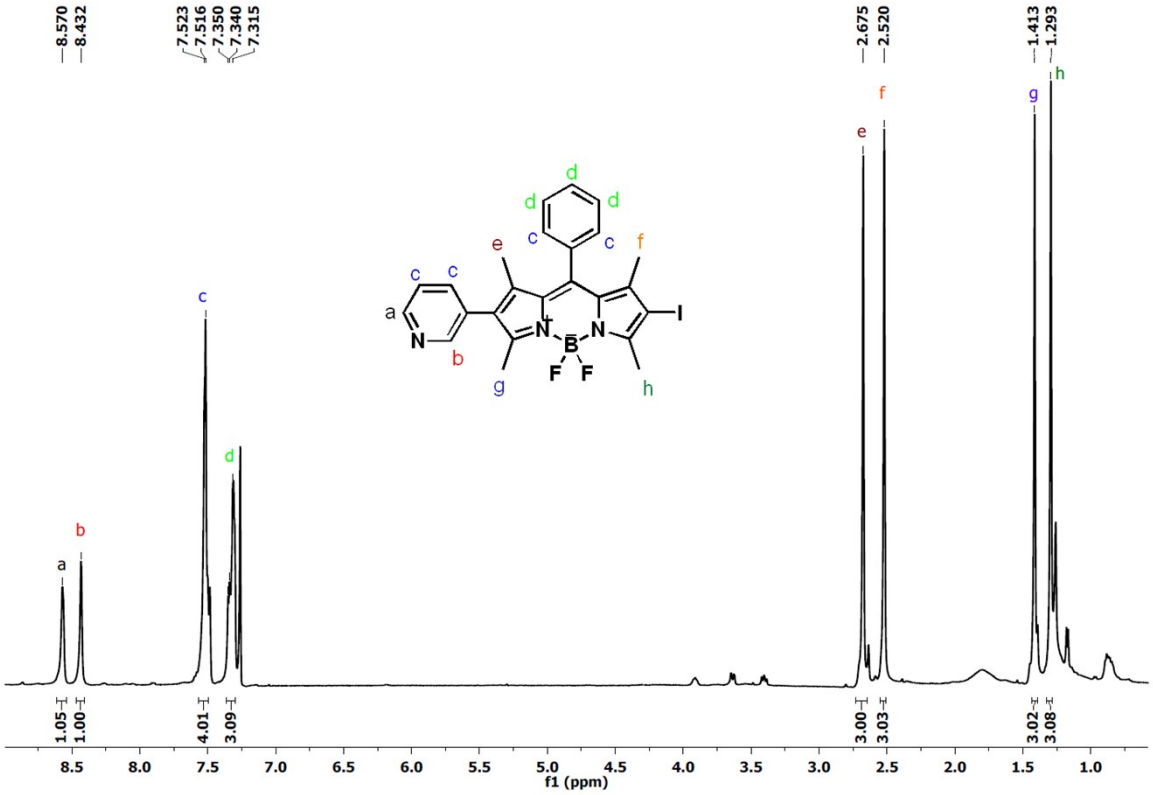

Figure S16. ^{1}H NMR Spectrum of Compound **B-3**

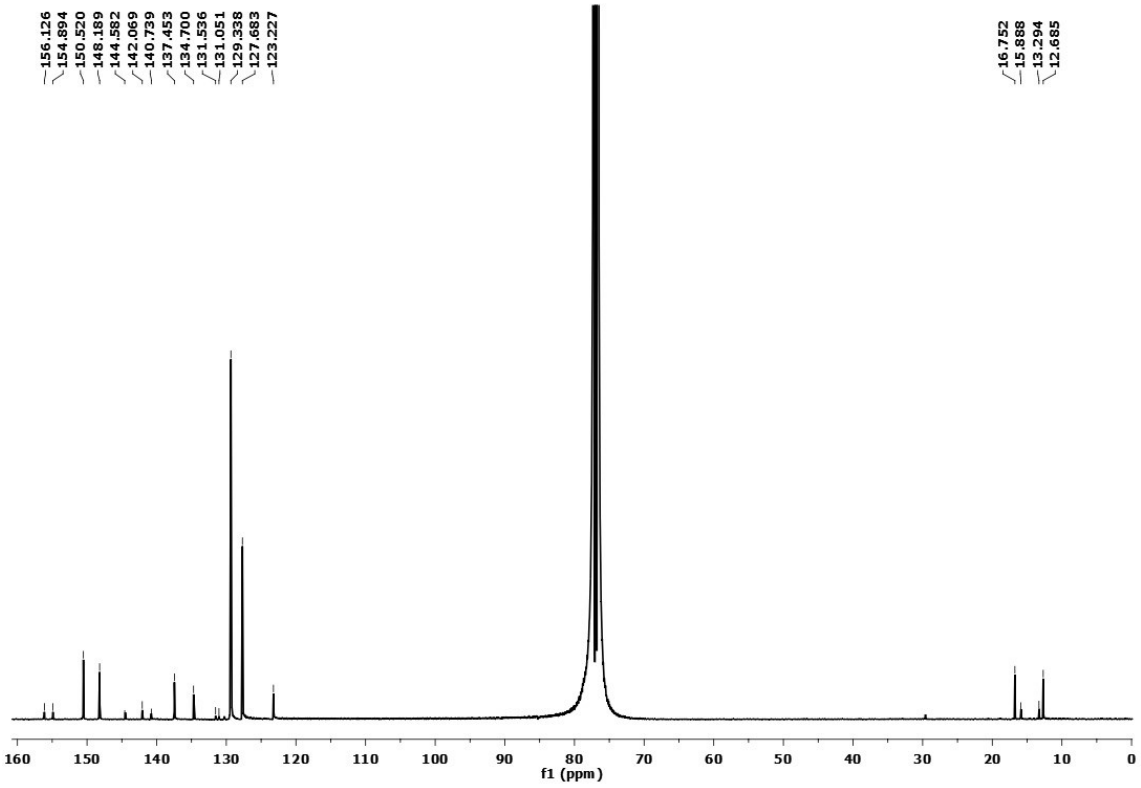

Figure S17. ^{13}C NMR Spectrum of Compound **B-3**

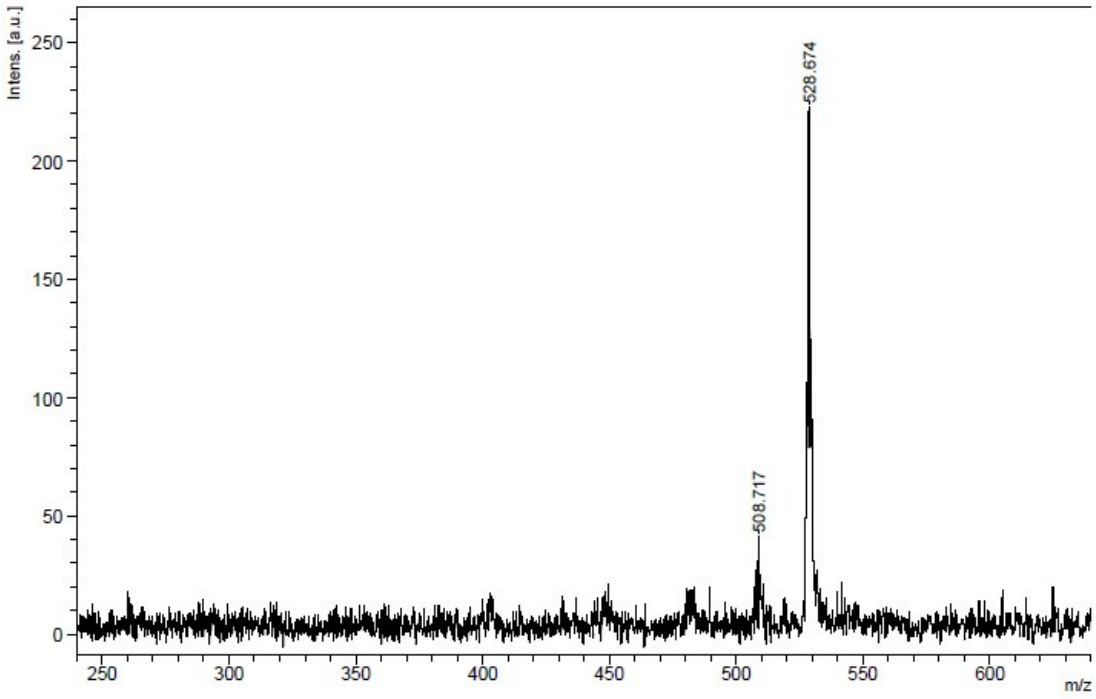

Figure S18. Mass Spectrum of Compound **B-3**

Table S2: The intermolecular D-H···A interaction parameters (Å and °) for BODIPY compounds.

D-H···A	Symmetry	d(D-H)	d(H···A)[1]	d(D-H···A)	D-H···A
B-2					
C23-H23···F2	1655.01	0.93	2.588	3.228	126.43
C46-H46···F1	2665.03	0.93	2.506	3.338	148.10
C35-H35A···F1	-	0.96	2.474	2.755	96.54
C35-H35C···F1	-	0.96	2.575	2.755	90.45
C15-H15···F2	2656.01	0.96	2.650	3.366	134.21
C47-H47···N5	2765.03	0.93	2.598	3.502	163.89
C45-H45···π1 (Cg2)	2665.01	0.93	2.554	3.088	116.70
C47-H47···π2 (Cg12)	2765.03	0.93	2.38	3.13(7)	137
B-3					
C35-H35A···F4	4575.02	0.96	2.551	3.508	173.72
C40-H40···F3	4575.02	0.93	2.508	3.262	138.30
C18-H18···F2	4565.01	0.93	2.492	3.284	143.32
C23-H23···N6	1565.02	0.93	2.645	3.489	151.14
C48-H48···π1 (Cg2)	4465.01	0.93	2.786	3.613	148.27

Table S3. Geometric parameters used for the determination of the π···π interactions*

Rings Cg(I)-Cg(J)[a]	Symmetry	Cg···Cg[b]	Cg(I)-Perp[c]	Cg(J)-Perp[d]	α[e]	β[f]	γ[g]
B-1							
Cg(1)···Cg(1)	x, 1-y, 1-z	4.3842(14)	3.8173	3.8172	0	29.5	29.5
B2							
Cg(1)···Cg(1)	1-x, -y ,1-z	4.489(5)	4.059(4)	4.060(4)	0.0(6)	25.3	25.3
Cg(1)···Cg(9)	1-x, 1-y, 1-z	3.946(9)	3.401(4)	3.830(8)	17.1(8)	13.9	30.5
Cg(2)···Cg(14)	1-x, 1-y, -z	4.13(2)	2.232(4)	3.82(2)	42	22.4	57.3
Cg(4)···Cg(7)	1-x, 1-y, 1-z	3.864(8)	3.795(4)	3.429(7)	16.7(8)	27.5	10.8
Cg(4)···Cg(11)	1-x, 1-y, 1-z	3.93(3)	3.772(4)	3.46(4)	12	28.1	16.1
Cg(7)···Cg(11)	2-x, 1-y, 1-z	4.55(3)	3.918(7)	4.00(3)	7	28.6	30.6
Cg(9)···Cg(11)	2-x, 1-y, 1-z	4.73(4)	4.319(7)	2.39(3)	48	59.7	24.1
Cg(12)···Cg(14)	2-x, 1-y, -z	4.31(5)	1.08(4)	4.07(2)	60	19.3	75.4
B-3							
Cg(4)···Cg(9)	x, y, z	4.062(7)	3.971(5)	3.174(4)	26.9(6)	38.6	12.2
Cg(9)···Cg(4)	x, y, z	4.061(7)	3.175(4)	3.970(5)	26.9(6)	12.2	38.6

* (Cg···Cg*b* < 5.0 Å). [a] In **B-1**, Cg(1) is the centroid of the pyrrole ring involving atoms N1-C1-C2-C3-C4. In **B-2,** Cg(1), Cg(2), Cg(4), Cg(7), Cg(9), Cg(11), Cg(12), and Cg(14) are the centroids of the rings N1-C4, N2-C9, N3-C17, N4-C67, N9-C64, N4-C33, N5-C31, and N6-C47, respectively. In **3**, Cg(4) and Cg(9) are the centroids of the rings N3-C24 and N4-C28, respectively.[b] Distance between ring centroids (Å).[c] Perpendicular distance of Cg(I) on ring J (Å).[d] Perpendicular distance of Cg(J) on ring I (Å).[e] Dihedral Angle between planes I and J (°).[f] Angle

between the centroid vector Cg(I)···Cg(J) vector and normal to plane I (°).[g] Angle between the centroid vector Cg(I)···Cg(J) vector and normal to plane J (°).

Hirshfeld surface analysis

Comparison of intermolecular interactions in B-1, B-2, and B-3

In order to get a better insight into the intermolecular interactions in BODIPY structures (**B-1, B-2**, and **B-3**), Hirshfeld surfaces[5] incorporating two-dimensional (2D) fingerprint plots[6] using Crystal Explorer[7] program was used. The normalized contact distance (d_{norm}) surface, which expressed in terms of distances to the surface from the nuclei inside and outside the Hirshfeld surface (d_i, and d_e, respectively) and the vdW radii of the atoms, defined as Eq. 1 gives identification of the regions of particular importance to intermolecular interactions.[8,9] The 2D fingerprint plots, which were derived from the combination of d_i, and d_e, were used for quantifying the intermolecular contacts in the crystal.

$$d_{norm} = \frac{d_i - r_i^{vdw}}{r_i^{vdw}} + \frac{d_e - r_e^{vdw}}{r_e^{vdw}} \qquad \text{Equation (1)}$$

Full fingerprint plots and their resolved fingerprint plots showing the percentage contributions to the total Hirshfeld surface area in **B-1**, **B-2**, and **B-3** are given in Figure S19, S20, and S21. Also, Figure S22 shows the relative percentage contributions of different intermolecular contacts contributing to the Hirshfeld surface. The 2D fingerprint plots exhibit that the most dominant interaction in **B-1**, **B-2** and **B-3** is the H/H interaction contributing to the total Hirshfeld surface with the values equal to 45%, 51.9%, and 49.7%, respectively. Unlike **B-2** and **B-3**, according to the 2D fingerprint plot **B-1**, the second most contribution to the total Hirshfeld surface in **B-1** is from I/H···H/I interactions appearing as distinct spikes, which constitute 20.4%. The C···H/H···C contacts representing C-H···π interactions comprise 12.9%, 15.6%, and 17.3% of the total

Hirshfeld surfaces for **B-1**, **B-2**, and **B-3**, respectively. As for the non-classical C-H···F hydrogen bonding interactions, these contacts are identified with the ratio of 3.5% (**B-1**), 12.9% (**B-2**), and 11.9% (**B-3**) of F/H···H/F in 2D fingerprint plots, and have an important role in the stabilization of 3D supramolecular network of **B-2** and **B-3**. With regard to the C-I···N XBs interactions, the I···N/N···I intermolecular interactions that represent XBs comprise 3.2% and 3.0% of the total Hirshfeld surfaces for **B-1** and **B-2**, respectively. On the other hand, **B-3** exhibits the I···F/F···I XBs interactions with the minor ratio of 1.4%. **B-1** and **B-3** do not show the close π–π stacking interactions (the C···C intermolecular interactions is smaller than 1% of the total Hirshfeld surfaces for both molecules) and also no exhibits the adjacent red and blue triangles on the shape index surface and also do not exhibit large flat region on the curvedness mapped on the Hirshfeld surface, as shown in Figure S23. For **B-2**, the C···C intermolecular interactions comprise 3.5% of the total Hirshfeld surface represent the aromatic π–π stacking ranging from 3.864(8) Å to 4.73(4) Å, as indicated in Table S3, between BODIPY molecules in crystal packing.

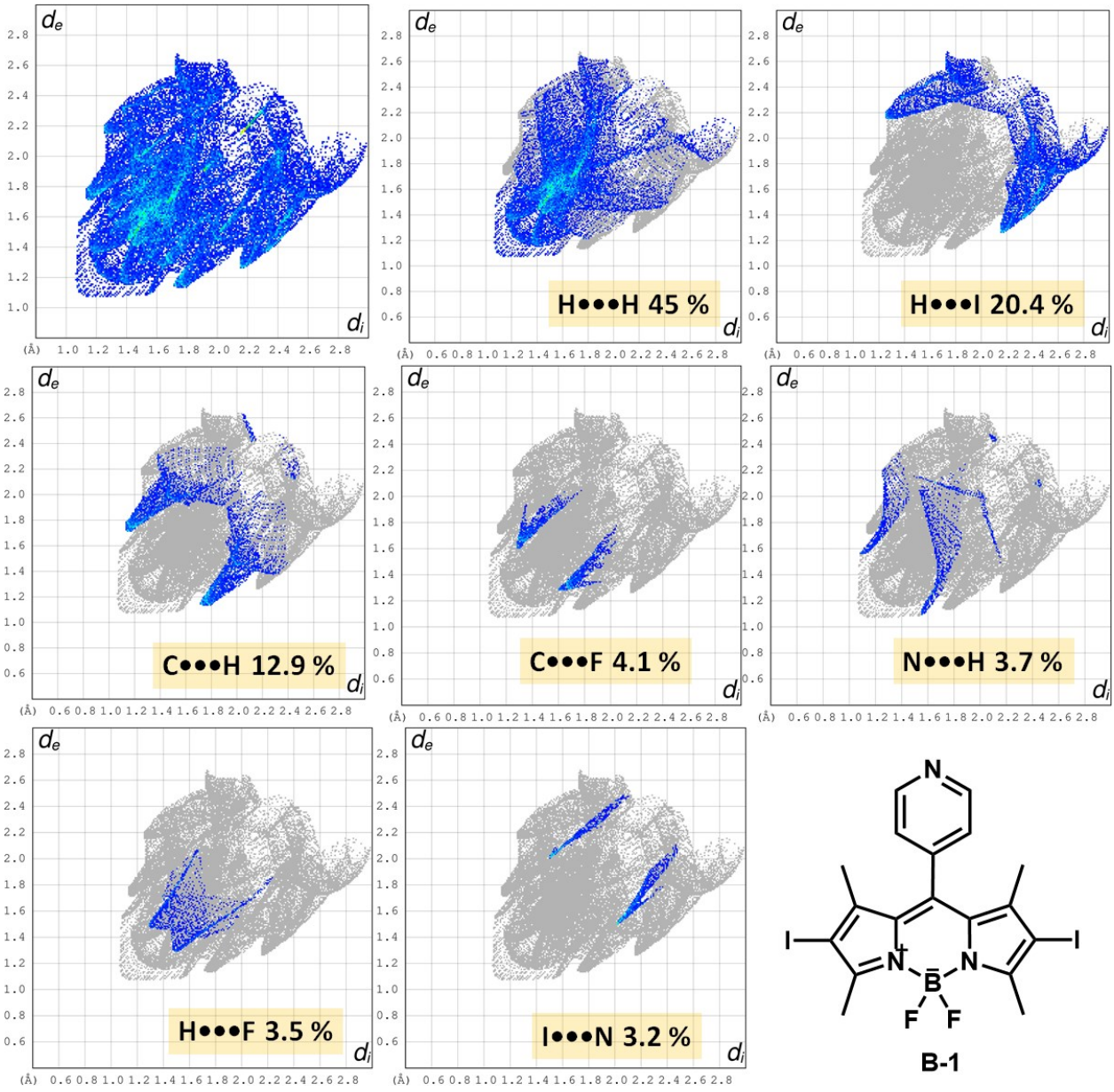

Figure S19. Full fingerprint plots and the resolved fingerprint plots showing the percentage contributions to the total Hirshfeld surface area in **B-1**.

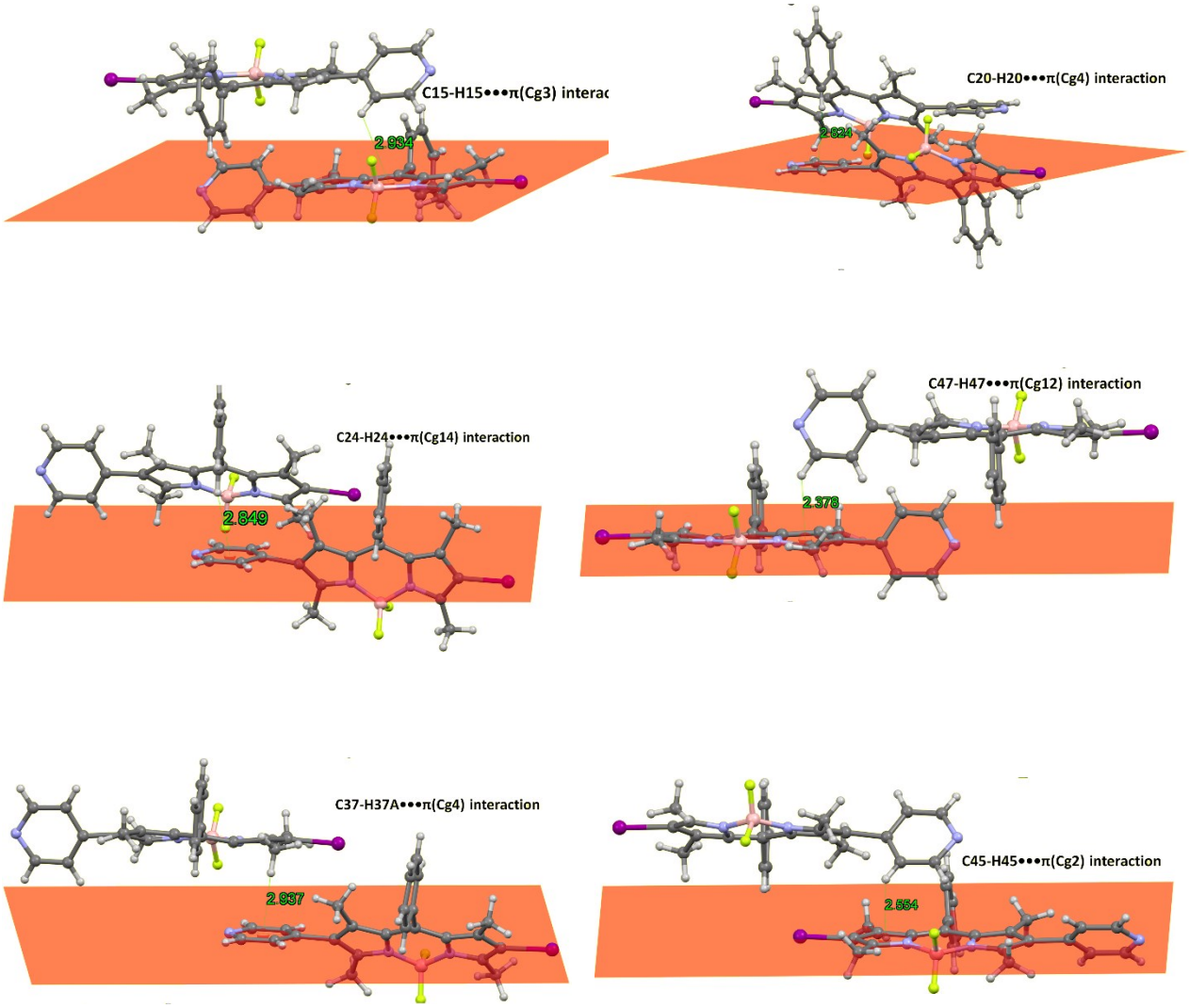

Figure S20. The weak C-H··· π_{BODIPY} interactions in **B-2**.

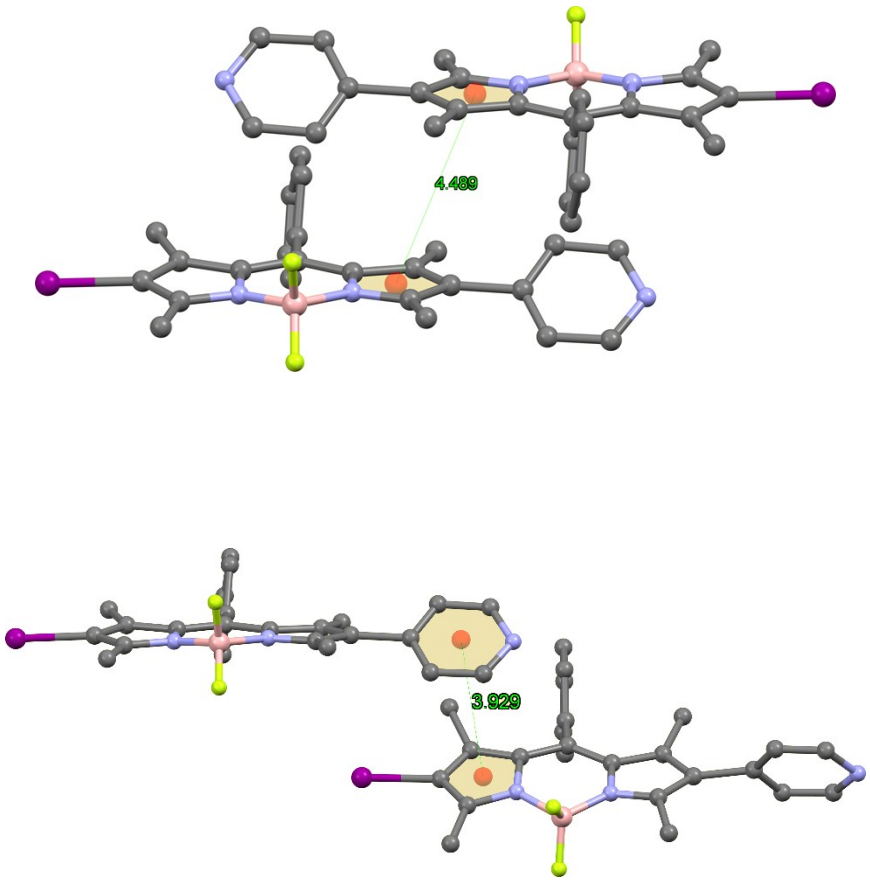

Figure S21. The π_{BODIPY} $\cdots\pi_{BODIPY}$ interactions in **B-2**.

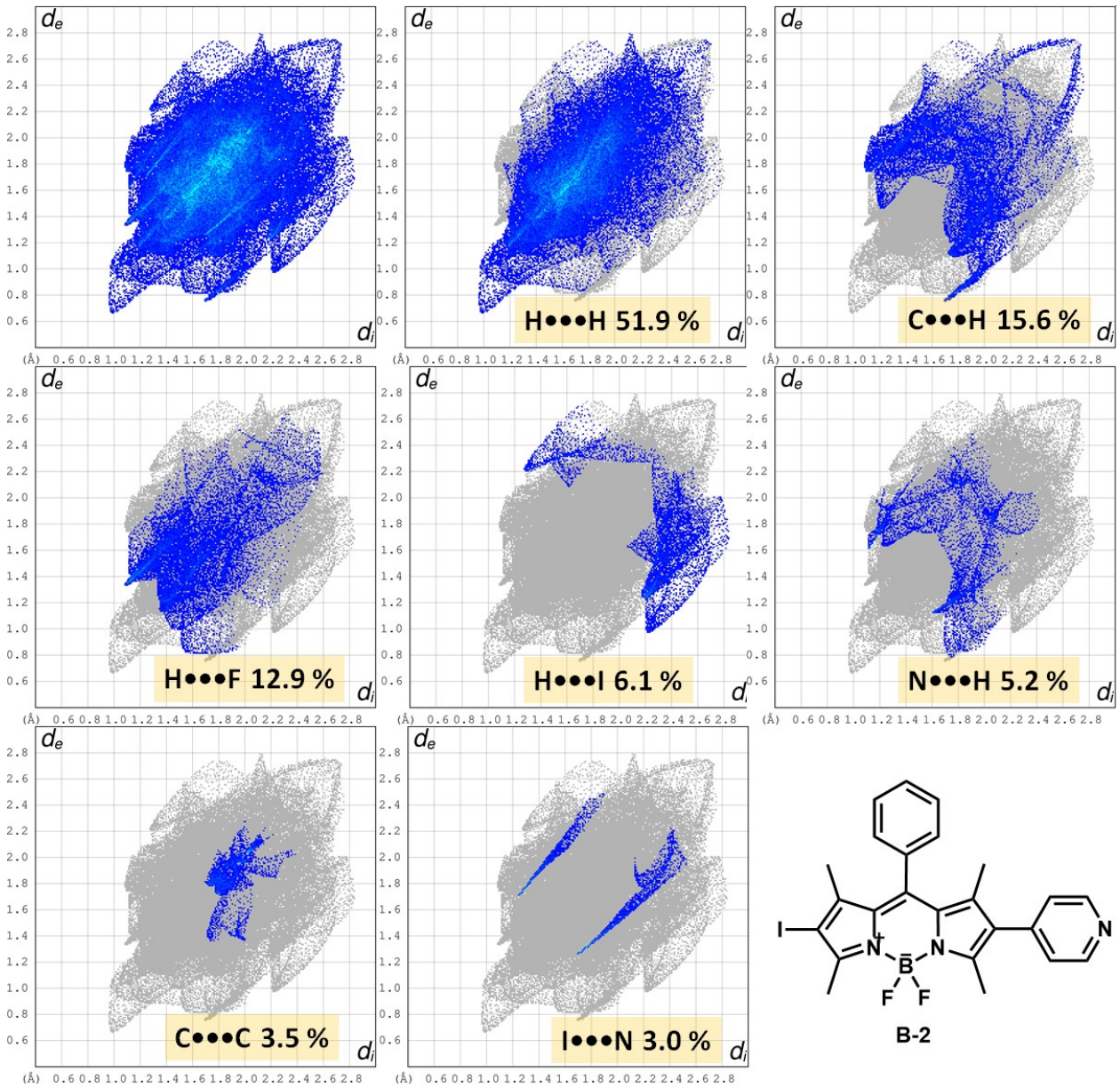

Figure S22. Full fingerprint plots and the resolved fingerprint plots showing the percentage contributions to the total Hirshfeld surface area in **B-2**.

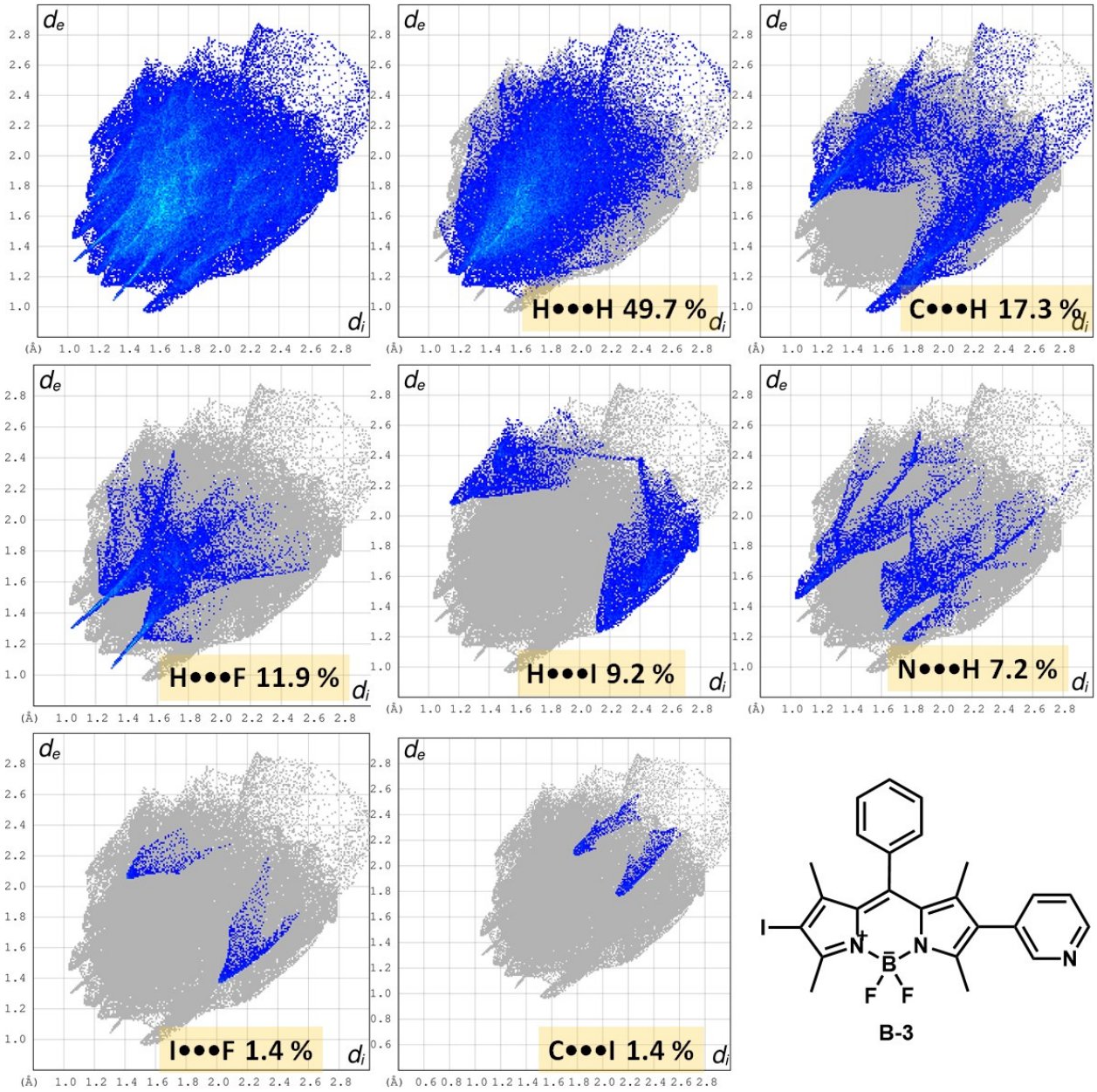

Figure S23. Full fingerprint plots and the resolved fingerprint plots showing the percentage contributions to the total Hirshfeld surface area in **B-3**.

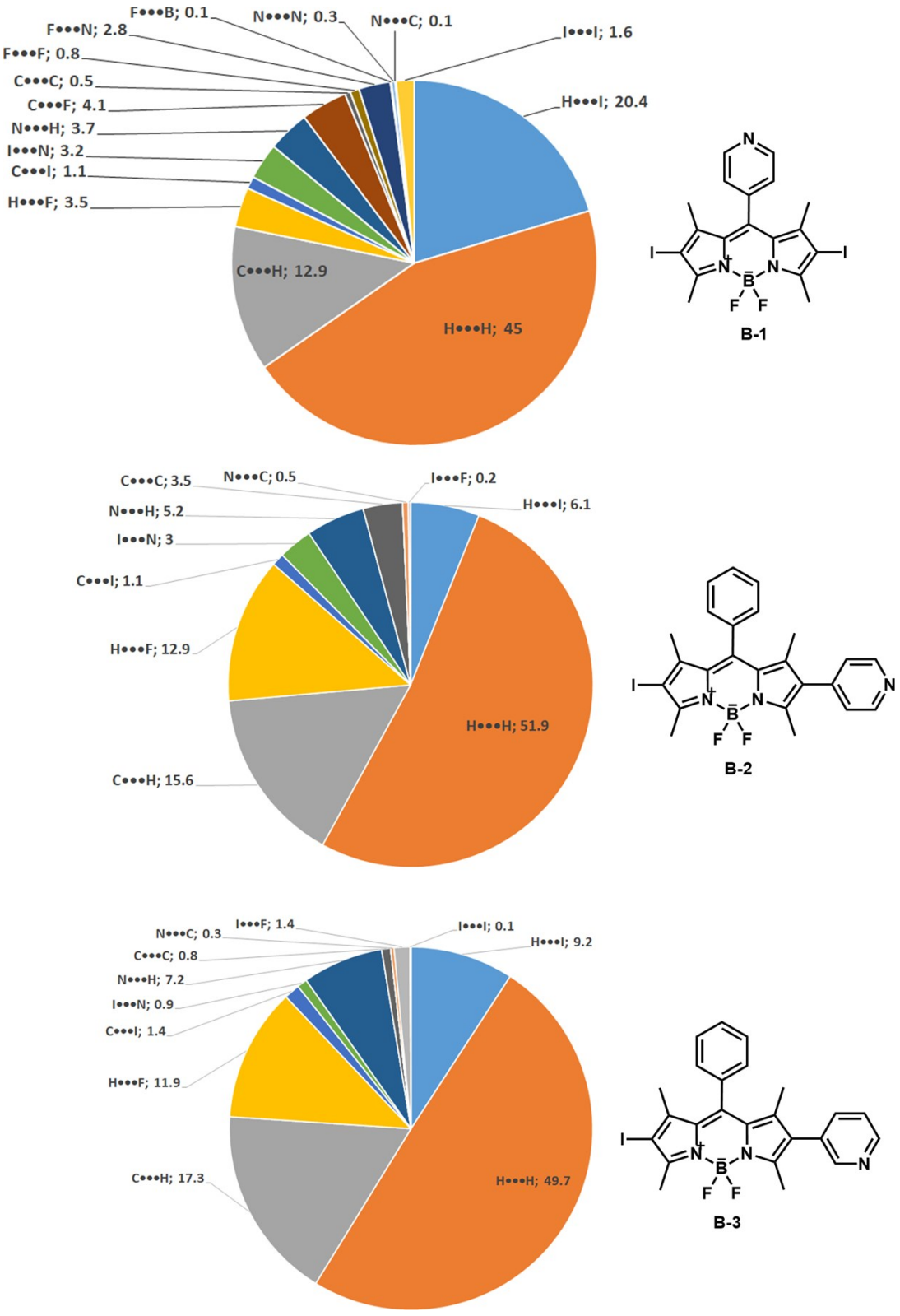

Figure S24. Relative percentage contributions of different intermolecular contacts contributing to the Hirshfeld surface in **B-1**, **B-2**, and **B-3**.

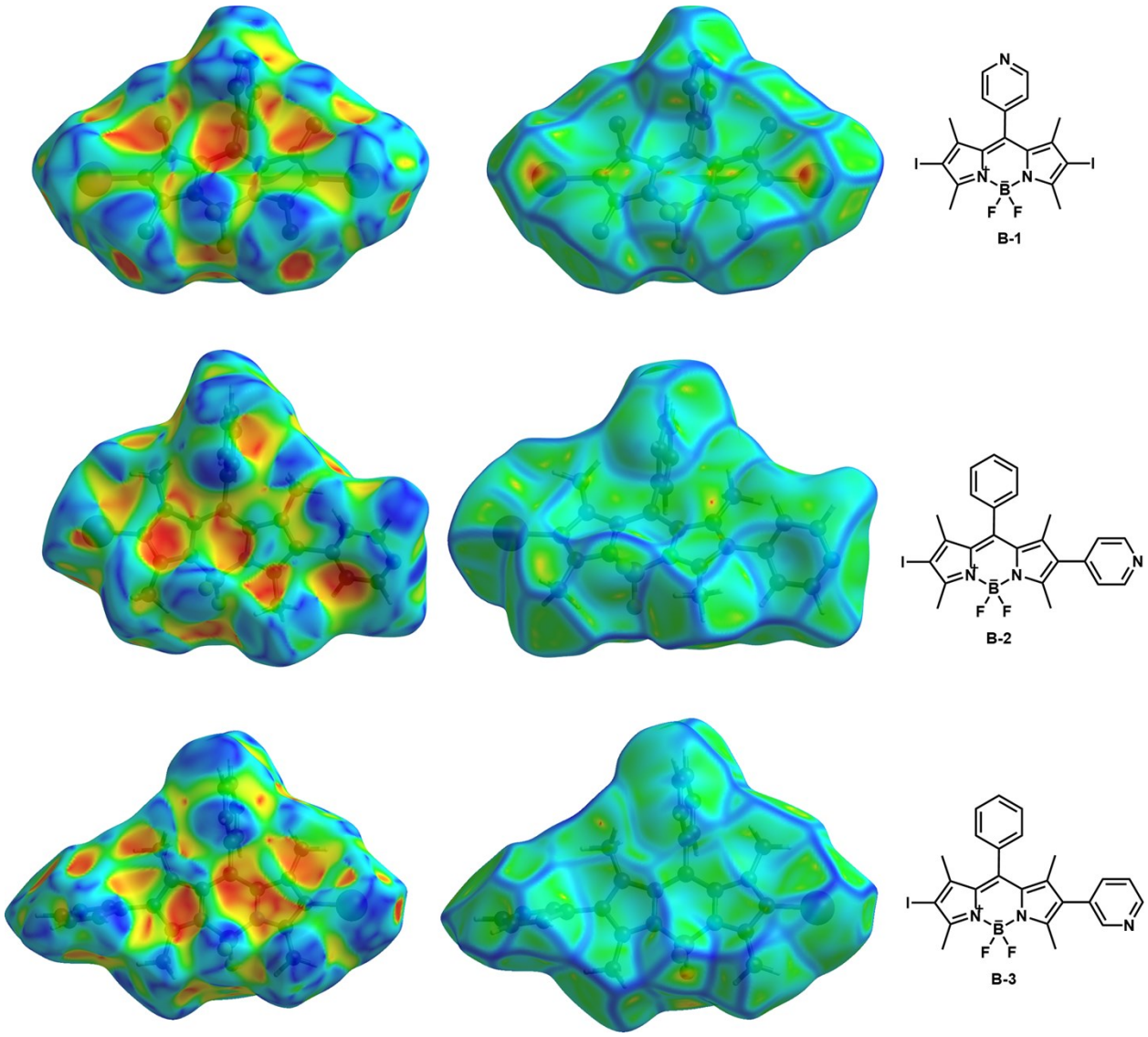

Figure S25. Perspective view of shape index (left) and curvedness (right)-mapped Hirshfeld surfaces in **B-1**, **B-2**, and **B-3**.

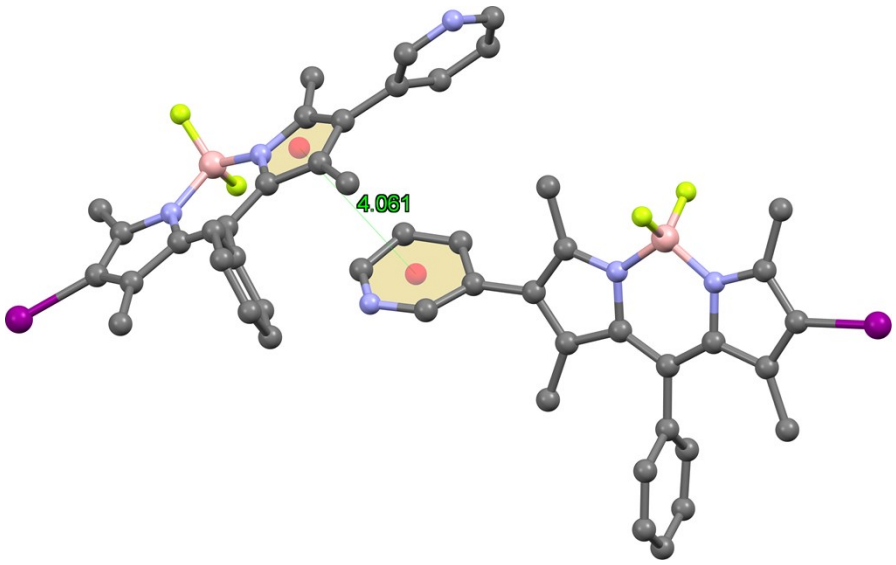

Figure S26. The π_{BODIPY} $\cdots\pi_{BODIPY}$ interactions in **B-3**.

Table S4. All BODIPY compounds containing I···F XB contacts in the Cambridge Structural Database (CSD) system.

CSD Ref. Code	REPRESENTATION	MOTIF	Ref.
CIMMUI01 CIMMUI03 CIMMUI04 CIMMUI05 CIMMUI06	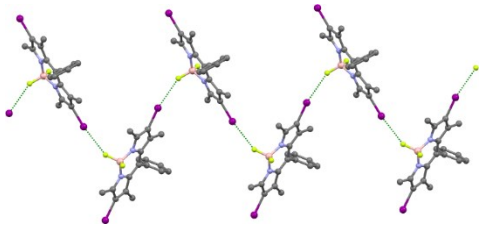	**1D ZIG-ZAG CHAIN**	10–14
CIMMUI02	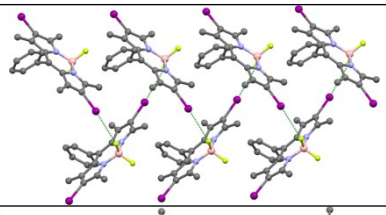	**1D HELIX**	15
BITSEE	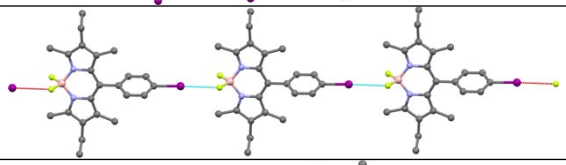	**1D LINEAR**	16
DANCAY	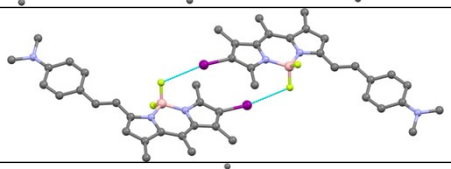	**0D DIMER**	17
HEZQEK	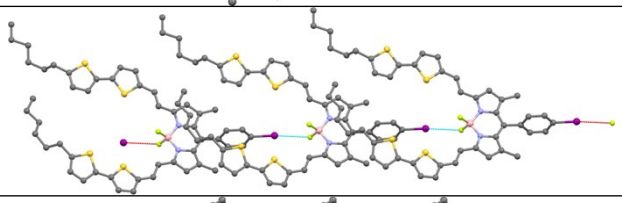	**1D LINEAR**	18
LACLEJ	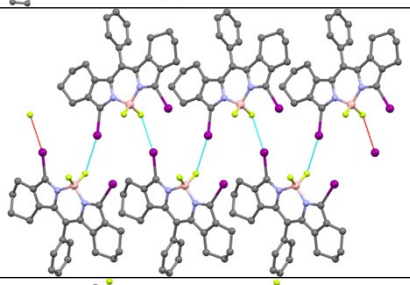	**1D ZIG-ZAG CHAIN**	19
YILZEA	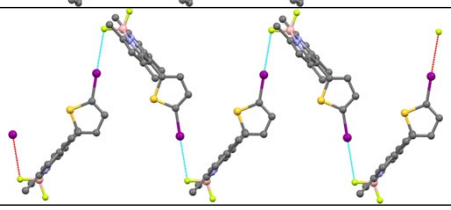	**1D ZIG-ZAG CHAIN**	20

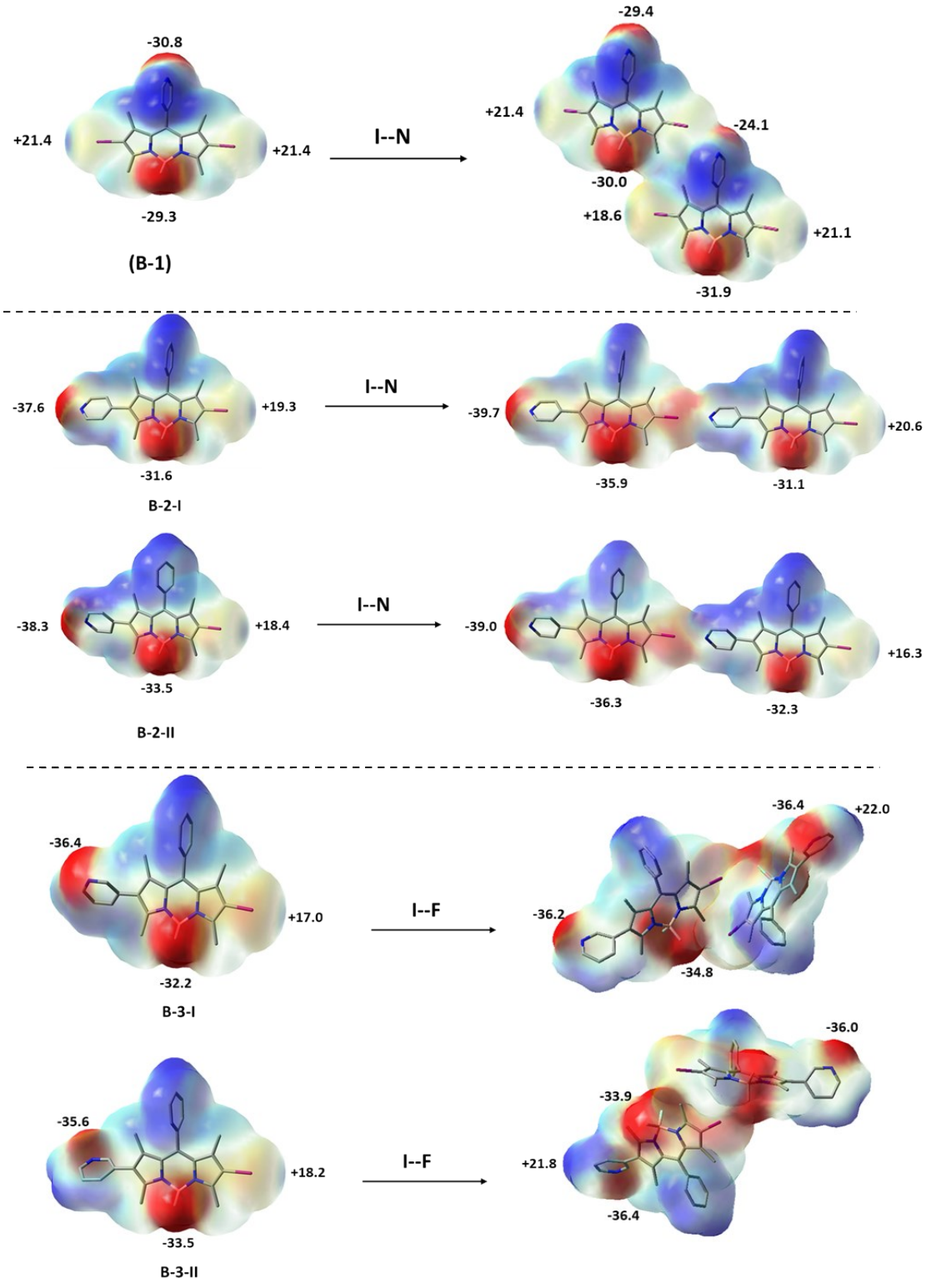

Figure S27. Electrostatic potential maps of XB dimer of **B-1**, **B-2(I**, **II)**, and **B-3 (I**, **II)** along with the corresponding electrostatic potential values (kcal/mol).

Table S5. Molecular orbital plots of the HOMOs and LUMOs of **B-1**, **B-2**, and **B-3**.

	HOMO	LUMO
B1	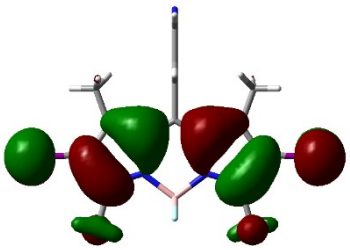	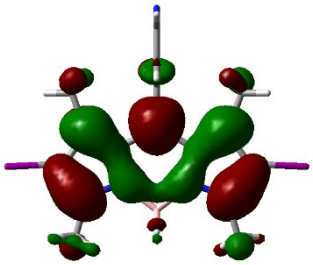
B2-I	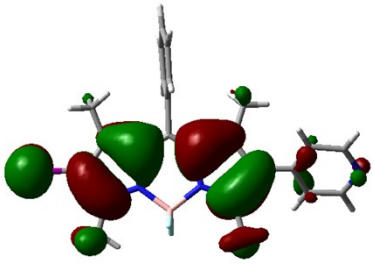	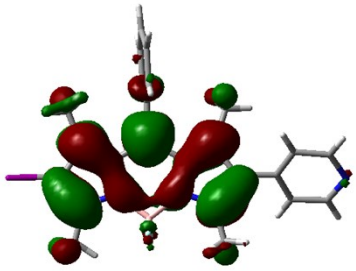
B2-II	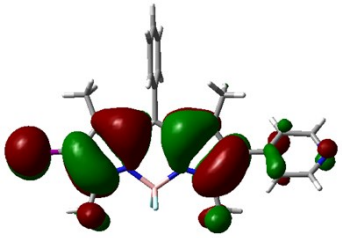	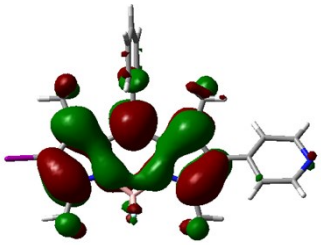
B3-I	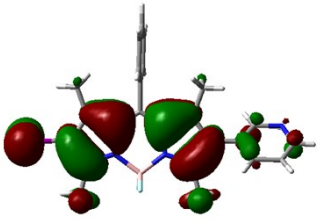	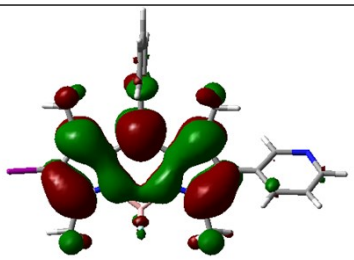
B3-II	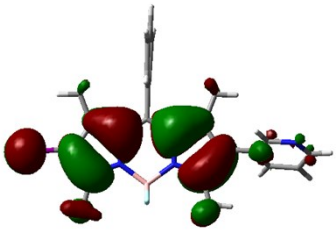	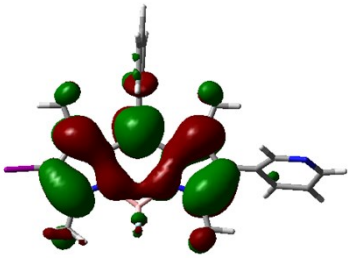

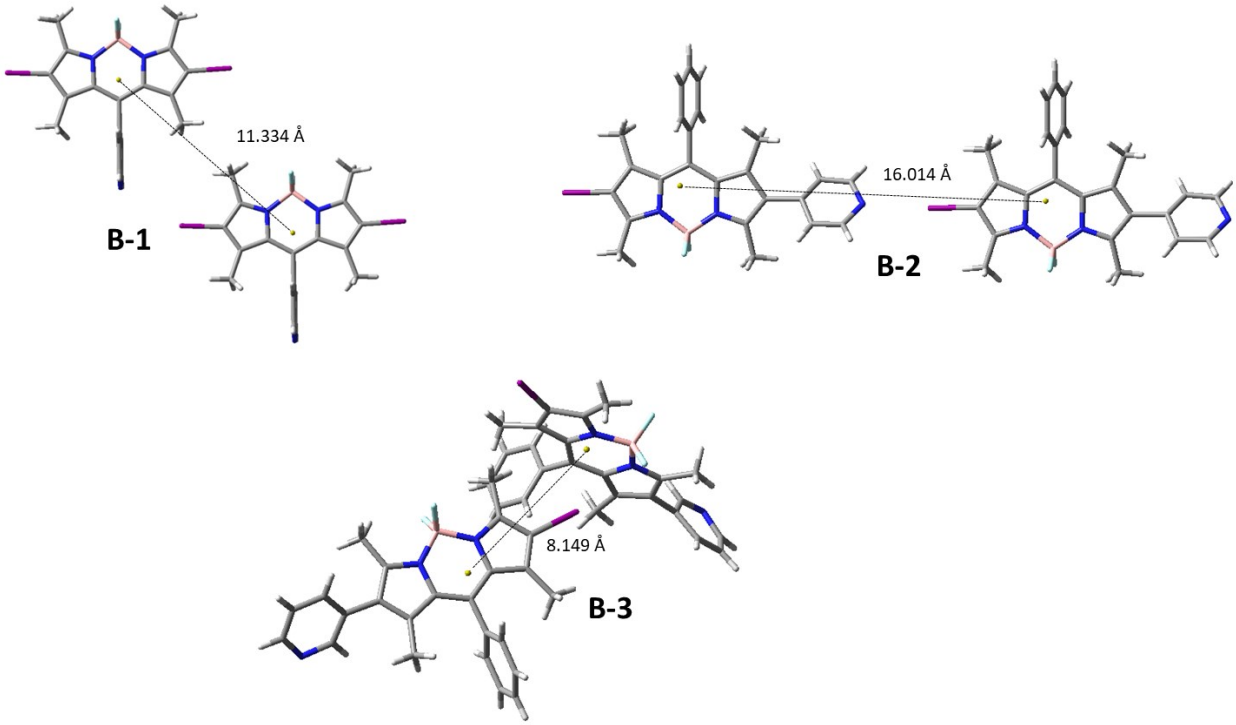

Figure S28. Centers of masses (shown as yellow spheres) in XB dimers of **B-1**, **B-2**, and **B-3.**

REFERENCES

1 G. Keşan, B. Topaloğlu, E. Özcan, H. H. Kazan, E. T. Eçik, E. Şenkuytu, I. F. Sengul, H. Kandemir and B. Çoşut, *Spectrochim. Acta - Part A Mol. Biomol. Spectrosc.*, 2019, **213**, 73–82.

2 W. Li, L. Li, H. Xiao, R. Qi, Y. Huang, Z. Xie, X. Jing and H. Zhang, *RSC Adv.*, 2013, **3**, 13417–13421.

3 D. Tian, F. Qi, H. Ma, X. Wang, Y. Pan, R. Chen, Z. Shen, Z. Liu, L. Huang and W. Huang, *Nat. Commun.*, 2018, **9**, 1–9.

4 G. G. Luo, K. Fang, J. H. Wu, J. C. Dai and Q. H. Zhao, *Phys. Chem. Chem. Phys.*, 2014, **16**, 23884–23894.

5 M. A. Spackman and D. Jayatilaka, *CrystEngComm*, 2009, **11**, 19–32.

6 M. A. Spackman and J. J. McKinnon, *CrystEngComm*, 2002, **4**, 378–392.

7 M. J. Turner, J. J. McKinnon, S. K. Wolff, D. J. Grimwood, P. R. Spackman,

D. Jayatilaka and M. A. Spackman, 2017.

8 J. J. McKinnon, M. A. Spackman and A. S. Mitchell, *Novel tools for visualizing and exploring intermolecular interactions in molecular crystals*, 2004, vol. 60.

9 J. J. McKinnon, D. Jayatilaka and M. A. Spackman, *Chem. Commun.*, 2007, 3814–3816.

10 J. H. Gibbs, L. T. Robins, Z. Zhou, P. Bobadova-Parvanova, M. Cottam, G. T. McCandless, F. R. Fronczek and M. G. H. Vicente, *Bioorganic Med. Chem.*, 2013, **21**, 5770–5781.

11 S. Swaminathan, C. Fowley, E. R. Thapaliya, B. McCaughan, S. Tang, A. Fraix, B. Captain, S. Sortino, J. F. Callan and F. M. Raymo, *Nanoscale*, 2015, **7**, 14071–14079.

12 J. Zhou, Y. Zhang, G. Yu, M. R. Crawley, C. R. P. Fulong, A. E. Friedman, S. Sengupta, J. Sun, Q. Li, F. Huang and T. R. Cook, *J. Am. Chem. Soc.*, 2018, **140**, 7730–7736.

13 M. Gorbe, A. M. Costero, F. Sancenón, R. Martínez-Máñez, R. Ballesteros-Cillero, L. E. Ochando, K. Chulvi, R. Gotor and S. Gil, *Dye. Pigment.*, 2019, **160**, 198–207.

14 H. Hassanain, E. S. Davies, W. Lewis, D. L. Kays and N. R. Champness, *Crystals*, 2020, **10**, 1–11.

15 R. P. Sabatini, B. Lindley, T. M. McCormick, T. Lazarides, W. W. Brennessel, D. W. McCamant and R. Eisenberg, *J. Phys. Chem. B*, 2016, **120**, 527–534.

16 E. Dubuisson, S. Badré, I. Gautier Luneau, G. Ulrich, J. P. Lemaistre, R. Pansu and A. Ibanez, *Dye. Pigment.*, 2013, **96**, 296–303.

17 S. Niu, G. Ulrich, P. Retailleau and R. Ziessel, *Org. Lett.*, 2011, **13**, 4996–4999.

18 T. Bura, N. Leclerc, S. Fall, P. Lévêque, T. Heiser, P. Retailleau, S. Rihn, A. Mirloup and R. Ziessel, *J. Am. Chem. Soc.*, 2012, **134**, 17404–17407.

19 Q. Meng, F. R. Fronczek and M. G. H. Vicente, *New J. Chem.*, 2016, **40**, 5740–5751.

20 A. Mirloup, P. Retailleau and R. Ziessel, *Tetrahedron Lett.*, 2013, **54**, 4456–4462.